

## 4. EXPERIMENTAL

### 4.1 VIAL EXPERIMENTS

#### *4.1.1 Solid Phase Micro Extraction (SPME)*

To obtain an initial profile of compounds in the headspace of the resin, a solid phase micro extraction (SPME) experiment was conducted. Oil-based resin (5.0 mL) was added to a clear 20 mL vial fitted with a septa cap. The cap was pierced with a SPME syringe containing a 100  $\mu\text{m}$  polydimethylsiloxane fiber (Restek Catalog # 27480-1). The selected fiber was recommended by the manufacturer to capture all volatiles with molecular weights between 60 g/mol and 275 g/mol, a range predicted to be suitable for this purpose. Once the syringe was securely fitted to the vial septa, the resin was exposed to 395 nm ultraviolet light provided by a handheld flashlight for 60 seconds, while the SPME fiber was exposed to the headspace. After light exposure, the fiber remained exposed to the vial headspace for another 360 seconds before being retracted into the syringe and removed from the vial. This experimental design is shown in Figure 15.

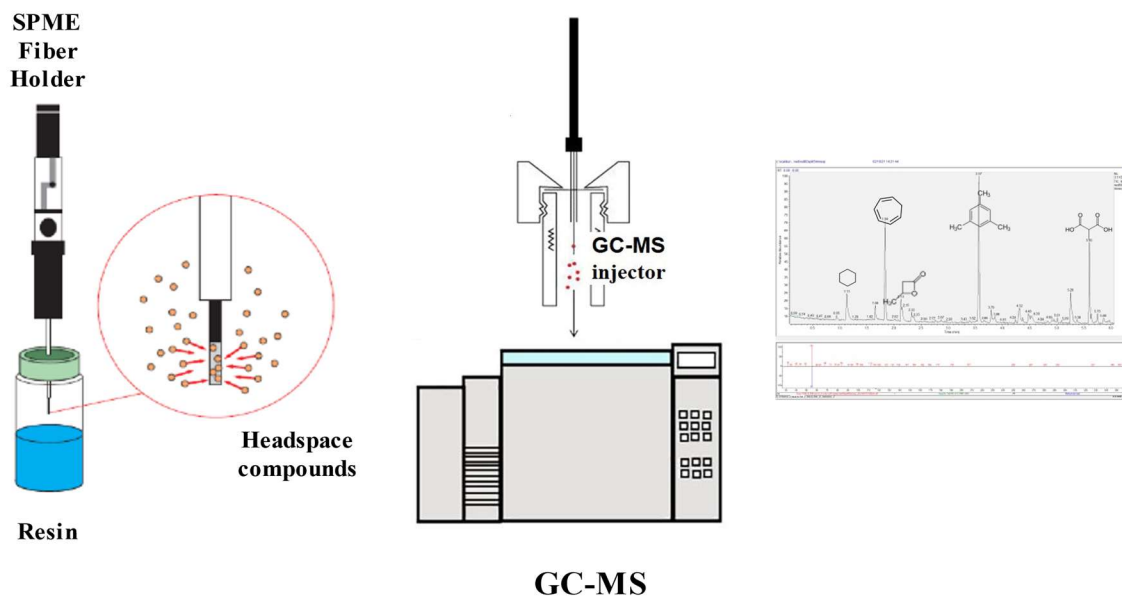


Figure 15: SPME Experimental design - SPME needle with fiber exposed inside of a glass vial.

#### 4.1.2 Chemical Analysis of SPME Fiber

Subsequent to exposure to oil-based resin headspace, the SPME syringe was transferred directly to the injection port of a Thermo Scientific Trace 1310 Gas Chromatograph (GC) coupled with a TSQ 8000 EVO Triple Quadrupole Mass Spectrometer (MS) and injected onto the head of a TG-5 SILMS column as shown in Figure 15. The split/splitless inlet was set to 250°C with a flow rate of 1.2 ml/min of ultrapure helium gas through the column. The GC oven ramp began at 50°C for 3 min and then increased by 12°C/min to 320°C and held for 5 min for a total run time of 30 min. The MS instrument was run in scan with a mass range of 35 to 650 m/z.

#### 4.2 ENCLOSURE EXPERIMENTS

To scale the initial vial experiments to suit the scope of this body of work, a 315-liter enclosure was constructed using Chemcast Cast Acrylic from TAP Plastics in Sacramento California. Compression fitting ports were installed on either side of the enclosure to facilitate sampling; this experimental set up shown in Figure 16.



**Figure 16: Enclosure, 315 Liters. (.94m x .66m x .66m)**

#### *4.2.1 mSLA Printer*

For the work presented in this thesis, the Anycubic Photon mSLA<sup>13</sup> printer was used to generate the volatile compounds of interest. Figure 17 provides a closer look at this instrument and Figure 18 shows it inside the constructed enclosure.

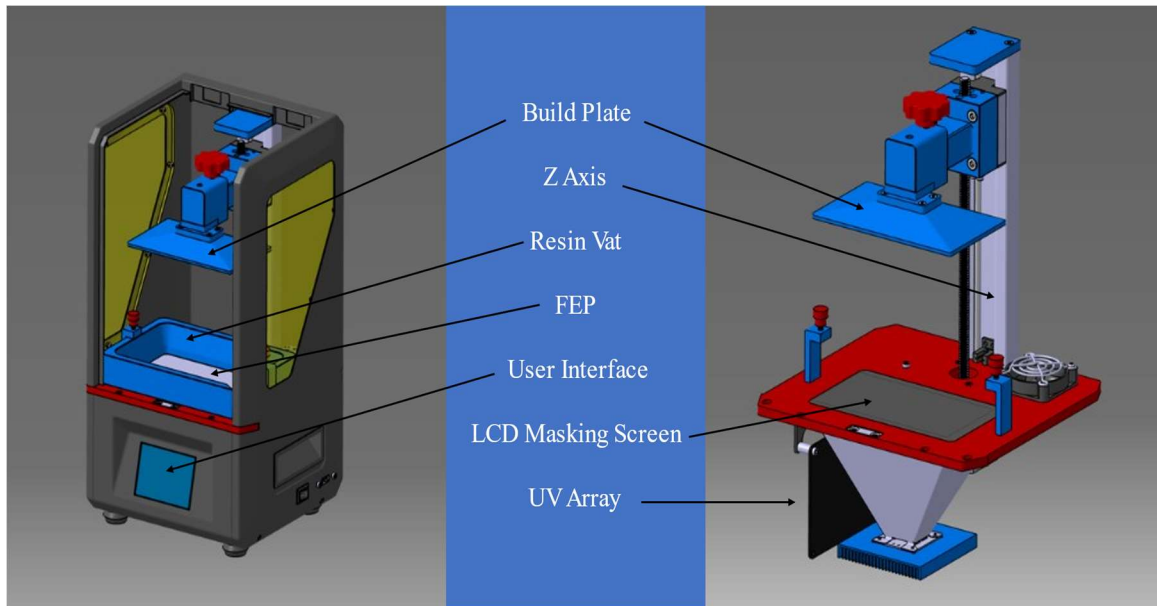


**Figure 17: 3D schematic of the Anycubic Photon.**



**Figure 18: Printer in the enclosure.**

The experimental process created for this thesis can be simplified into a small number of steps shown in the scheme presented in Figure 19.

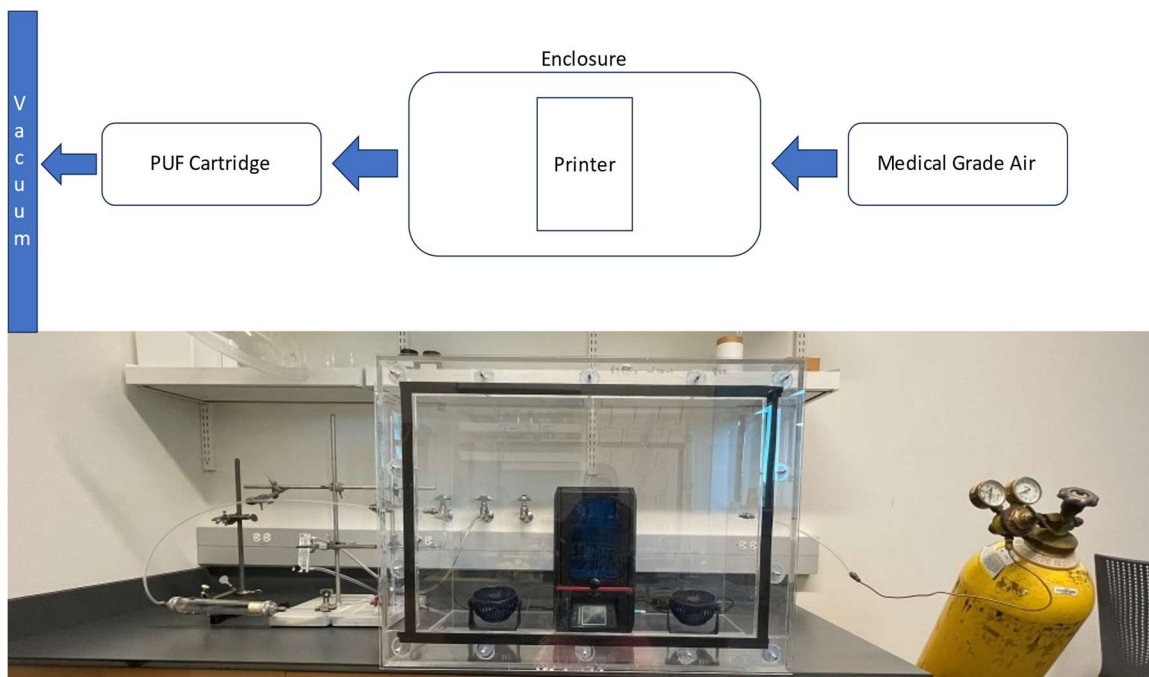


Figure 19: Flow chart of the experimental process.

The resin vat was filled to the operational limit of 200 mL. A model was chosen from the attached electronic storage device and the build plate lowers into the resin bath for the first exposure. The base layers are responsible for the strength of the bond between the build plate and the object, and so take longer to print than subsequent, “normal” layers. Though these layers are the same layer height, the extra cure time creates a hold that ensures that the print does not detach mid experiment. Once the base layers have been completed, normal layers begin and continue until the model is completely fabricated. The printing time required depends on the size of the model and the printing parameters programmed (e.g., layer height).

#### 4.2.1.1 Experimental Printing Parameters

The printing parameters are tabulated below in Table 6.

**Table 6: Anycubic photon printing parameters.**

<b>Layer Thickness (mm)</b>	<b>Layer Exposure Time (s)</b>	<b>Bottom Layers</b>	<b>Bottom Layer Exposure Time (s)</b>	<b>Resolution (Pixels)</b>
<b>0.03</b>	9	20	90	1440 x 2560

Object choice

Two shapes were chosen for this research, the parameters of which are shown in Table 7.

**Table 7: Shapes chosen and associated dimensions.**

<b>Shape</b>	<b>Surface Area (mm<sup>2</sup>)</b>	<b>Calculated Volume of Resin Used (mL)</b>
<b>Cube</b>	9240	31.0
<b>Square Pyramid</b>	15200	31.0

These were chosen to determine if objects with differing surface area, same total volume (and mass), result in different VOC emission rates. The equations used to determine the surface areas is shown below.

**Equation 1: Area of a Cube.**

$$A = 6a^2$$

**Equation 2: Area of a Square Pyramid.**

$$A = a^2 + 2a \sqrt{\frac{a^2}{4} + h^2}$$

The plate configurations for the prints studied are shown in Figures 20 and 21 below.

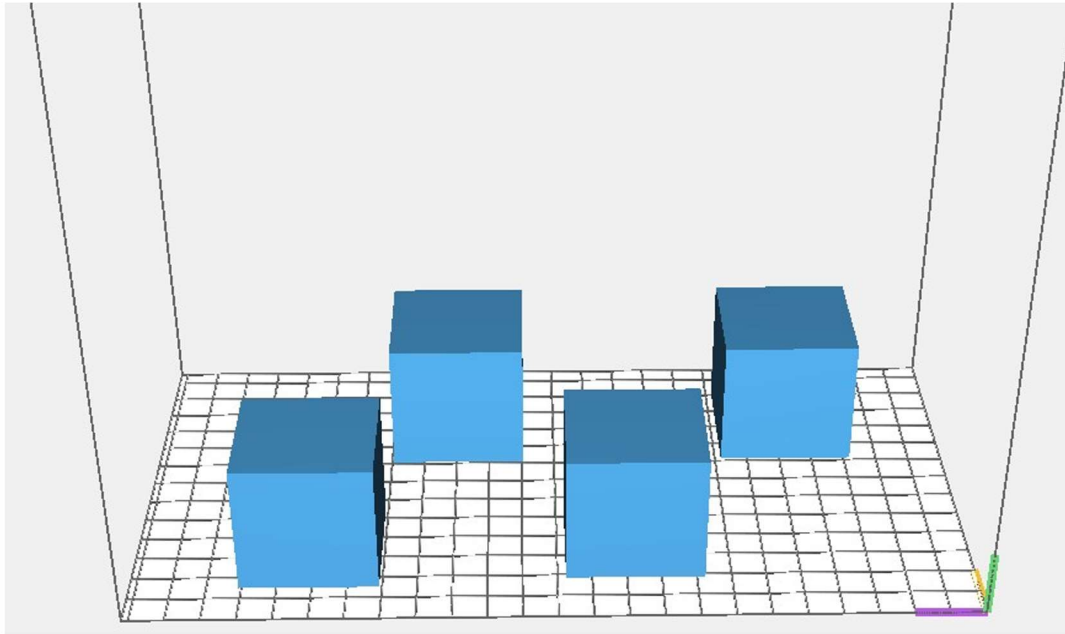


**Figure 20: Build plate configuration for Cube experiments.**

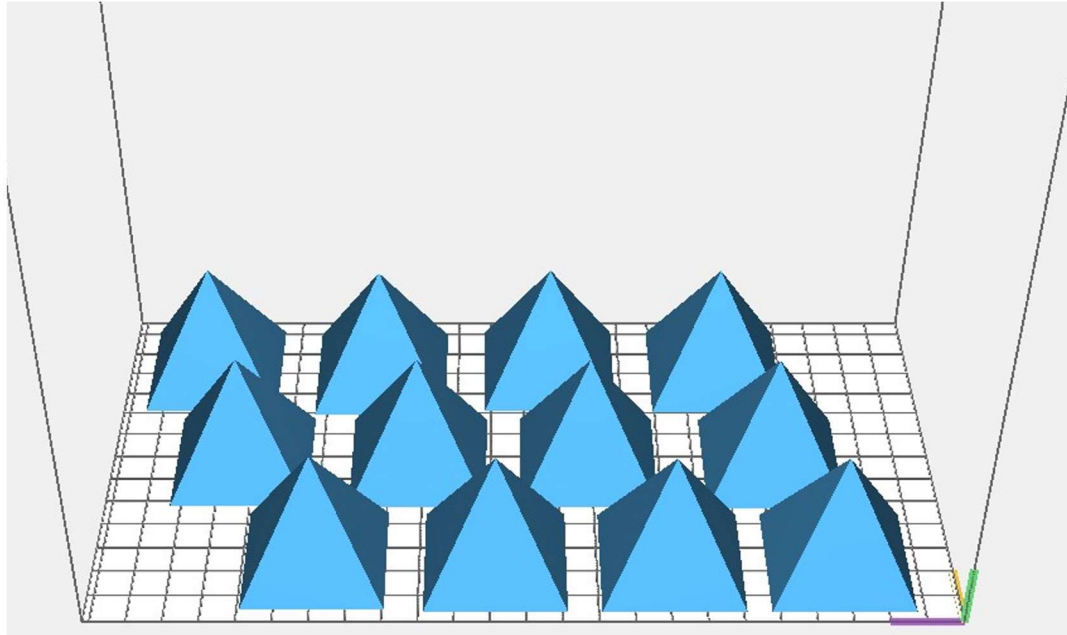


**Figure 21: Build plate configuration for Square Pyramid experiments.**

#### *4.2.2 Resin Choice*

Two photopolymer resins were chosen for this body of work to examine the difference in emission profile: Anycubic Clear<sup>23</sup> and Anycubic Eco Clear<sup>24</sup>. Both were investigated using the same printing parameters to minimize any variables that might produce differing results based on experimental procedure. The appearance of the liquid resin is shown in Figure 22.



**Figure 22: Anycubic resins in beakers, oil-based on the left and plant-based on the right.**

#### *4.2.3 Post Processing Instrument*

Although curing can be done manually, the post processing can be performed by commercially available instruments. The Anycubic Wash & Cure (ASIN B08JCSSTD1) was chosen as the post processing instrument for this work to eliminate any user bias in the handling of the experiment. This instrument is shown in Figure 23.



**Figure 23: Anycubic wash & cure.**

The build plate is transferred directly from the printer to the wash and cure, where it is submerged in a bath of isopropyl alcohol as shown in Figure 24.



**Figure 24: Build plate transferred from the printer to the wash & cure.**

#### 4.2.3.1 Post-Processing Parameters

The post processing parameters are determined by the size of the object fabricated in the during phase. Larger objects require longer washes to rinse the unreacted photopolymer resin from the surface, and longer cure times to account for the increased volume. Complicated geometries also benefit from longer wash and cure cycles to ensure a complete post processing. Since the objects printed for this study are geometrically unsophisticated, the post processing phases were brief, 60 seconds for the wash cycle, and 5 minutes for the final cure.

#### 4.2.4 Sampling Manifold

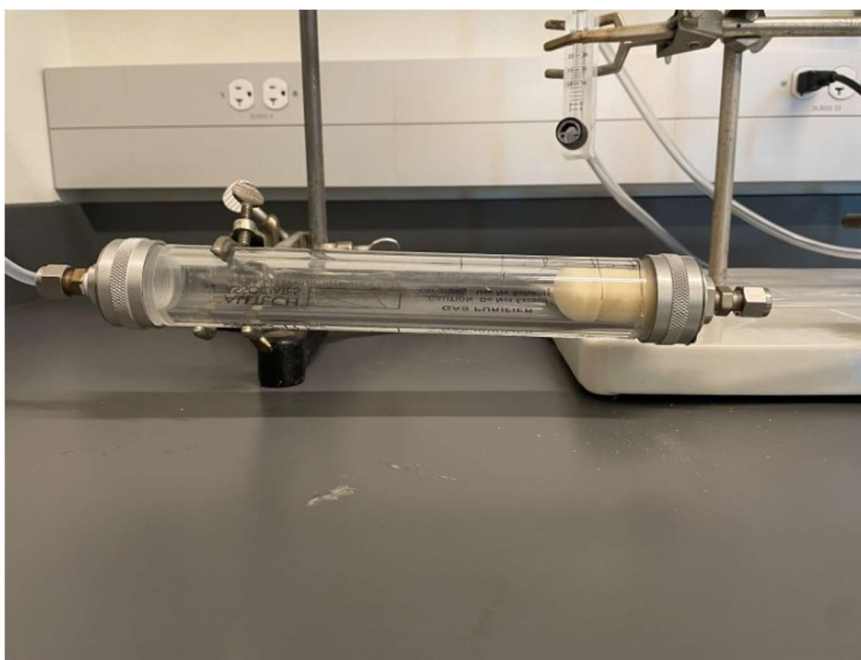
A Swagelok manifold was attached to the side of the enclosure to capture the gas phase analytes and is shown below in Figure 25.



Figure 25: Swagelok manifold, flow path indicated.

#### 4.2.4.1 Polyurethane Foam Cartridge (PUF) Sampling Media

Polyurethane Foam (PUF) (Tisch TE-1011) was chosen as the primary medium for capturing the emission. Several US EPA methods using PUF are well established and have been shown to be effective in collecting pesticides and volatile organic compounds.<sup>25</sup> Medical grade air was pulled through the compression fitting manifold via vacuum at a rate of 30 L/min for 60 min to ensure at least 5 full box changes. The loaded PUF cartridge is shown in Figure 26.



**Figure 26: PUF cartridge loaded with a PUF.**

### 4.3 EXTRACTION OF PUF SAMPLING MEDIA

Once the gas-phase emissions were collected onto the PUF medium via the manifold, the PUF was submerged in 125 mL of dichloromethane and sonicated for 60

minutes. To ensure complete extraction, the PUF was extracted two more times and these extracts were analyzed for carry over. An overlaid set of chromatograms showing this experiment is presented below in Figure 27.

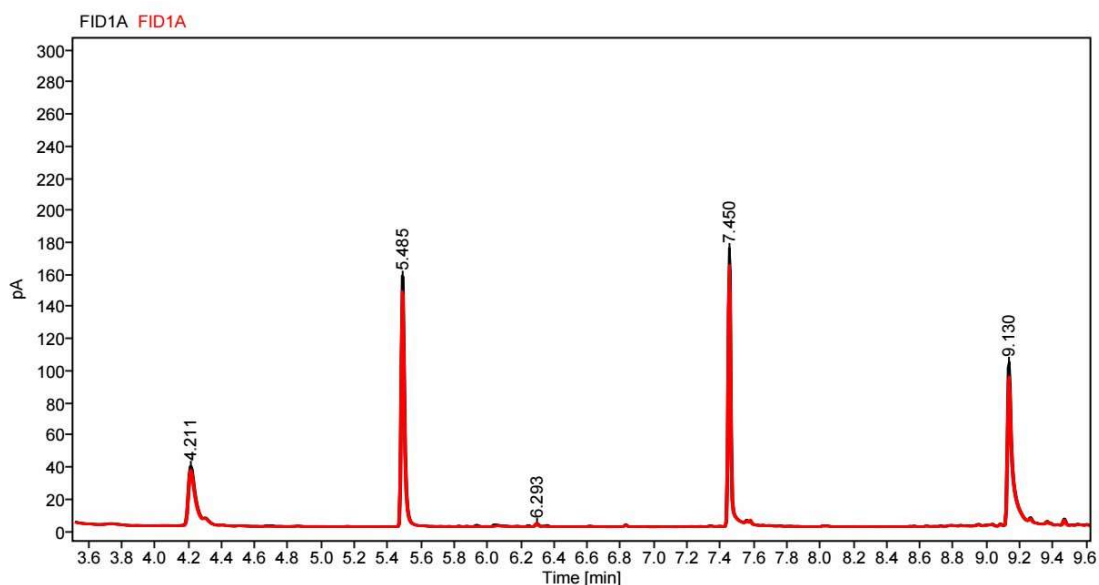


Figure 27: Overlaid chromatograms of the second (red) and third PUF extraction (black).

After sonication, the extract was subjected to various dilutions: An unconcentrated sample, where an aliquot was taken directly from the extract (termed the [U] extract), a dilution where 12.5 mL was taken from the extract, concentrated to 1000  $\mu\text{L}$ , then 200  $\mu\text{L}$  was put into an autosampler vial for analysis (termed the [1000] extract), and a dilution where 12.5 mL were taken from the extract, concentrated to 200  $\mu\text{L}$  and then transferred to an autosampler (termed the [200] extract). A scheme of this process is illustrated below in Figure 28. These extractions were performed to ensure that each analyte would be within the calibration range in at least one of the concentration levels.

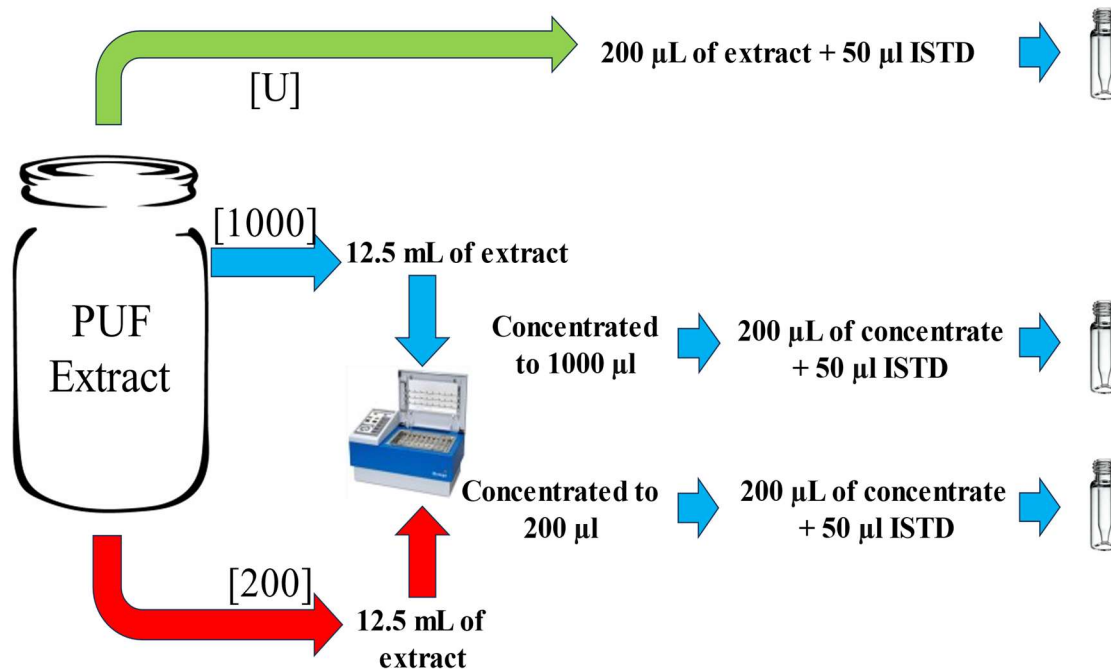


Figure 28: Concentration scheme for [U], [1000] and [200] levels.

#### 4.4. QUANTIFICATION AND QUALITY ASSURANCE/ QUALITY CONTROL (QA/QC)

##### 4.4.1 Internal Standards

To correct for variability in instrument response and evaporative concentration over long sequence analyses, internal standard calibration was employed. A mixture of deuterated polycyclic aromatic hydrocarbons contained in RESTEK Revised SV Internal Standard Mix (Restek 31885) was added to each sample and calibration standard. A single component of this mixture, d10-phenanthrene was used as the internal standard.<sup>26</sup>

#### 4.4.2 Calibration Curves

The calibration curves for the six VOC analytes spanned a nominal range of 0.05 µg analyte/mL extract-1250 ug/mL extract. The specific calibration range for each analyte was dictated by linearity and accuracy thresholds and was consistent over the analysis batches from which data presented in this work is presented.

**Equation 3: Internal Standard Ratio equation.**

$$\text{Peak Area} \div \text{ISTD Peak Area (d10 Phenanthrene)} = \text{Internal Standard Ratio}$$

**Equation 4: Concentration equation.**

$$\text{Concentration} = \frac{\text{ISTD Ratio} - y \text{ intercept (cal curve)}}{\text{slope (cal curve)}}$$

This ensured all responses were normalized to the known internal standard amount. Only curves with a R<sup>2</sup> value of 0.98 or better were considered. All curves had an average accuracy within 95% and 105%, and 1/x (inverse concentration) weighting was applied to the linear regressions.

**Equation 5: Accuracy equation.**

$$(\text{Experimental Concentration} \div \text{Expected Concentration}) \times 100 = \% \text{ Accuracy}$$

Only peaks with a signal to noise (S/N) value greater than 10 were used in the regression or were used to generate concentration data. The S/N was based on peak height

signal and the root mean square (RMS) noise from a period of 0.4 minutes before or after the peak of interest.

#### *4.4.3 Control Checks*

Recovery experiments for each analyte were included to investigate the impact of sonication and concentration via evaporation. Using a high-level calibration standard, three different dilutions were prepared in the same manner as the sample dilutions described in Figure 28: [U], [1000] and [200].

#### *4.4.4 Limit of Detection*

The limit of detection for each analyte was calculated using the following equation.

**Equation 6: Limit of detection equation.**

$$LOD = S_y \times \frac{3.3}{m}$$

Where  $S_y$  = Standard Deviation of the analyte calibration curve

$m$  = Slope of the calibration curve

Though there are many different ways to calculate the LOD, Equation 6 was well suited for our experimental set up. Other common equations use the standard deviation of blank contamination peaks, or low-level spikes to determine an MDL. Since we observed no blank contamination, and this is not a regulatory experiment, both were not considered. Analyte concentrations that were below the LOD were not included in the averaged results presented in this work.

#### *4.4.5 Method and Enclosure blanks*

To determine background contamination or interferences in the analytical system, a series of method and enclosure blanks were run with each analytical batch.

#### 4.5 ENCLOSURE EXPERIMENTAL ANALYSIS VIA GC-FID

All enclosure experiments were analyzed on an Agilent Intuvo Gas Chromatograph 9000 fitted with a HP-5MS UI column and a flame ionization detector. The inlet was set to splitless with an injection volume of 1.0  $\mu\text{L}$ , and was set to 300°C with a flow rate of 2.5 ml/min of helium gas through the column. The GC oven ramp began at 50°C for 0.5 min and then increased by 20°C/min to 300°C and held for 3 min for a total run time of 16 min. The FID temperature was set to 300°C.

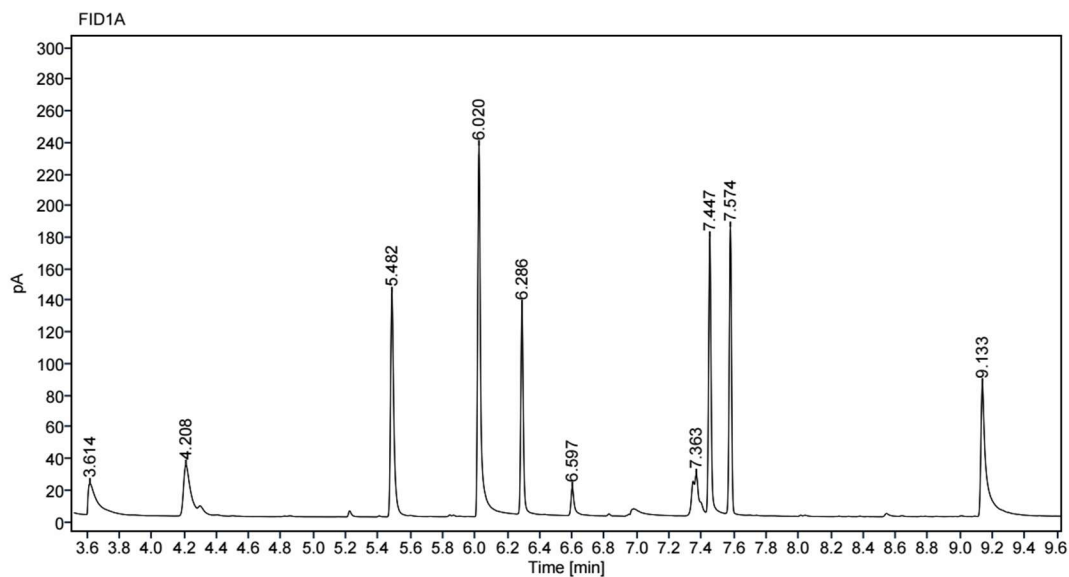
## 5. RESULTS

### 5.1 IDENTIFICATION OF ANALYTES

From the chromatographic peaks generated by the SPME experiment, mass spectra were extracted and candidate compounds were identified using the NIST17 mass spectral database. Based on this analysis, six compounds were identified. Each identification was verified against purchased standards, using retention times gathered on the Intuvo 9000 GC-FID and spectral data from the Trace 1310 GC-MS. Out of the seven major chromatographic peaks in the Total Ion Chromatogram from the SPME analysis, six compounds were identified. Figure 29 shows a TIC of a PUF extract with internal standards added.

Figure 29: Chromatogram of initial resin experiments. Internal standards: 1,4-Dichlorobenze-d4 (4.208), Napthalene-d8 (5.482), Acenaphthalened-d10(7.447), Phenanthrene d10(9.113)

#### 5.1.1 2-Hydroxyethyl Acrylate (2-HEA)



The structure of 2-HEA is shown below in Figure 30.

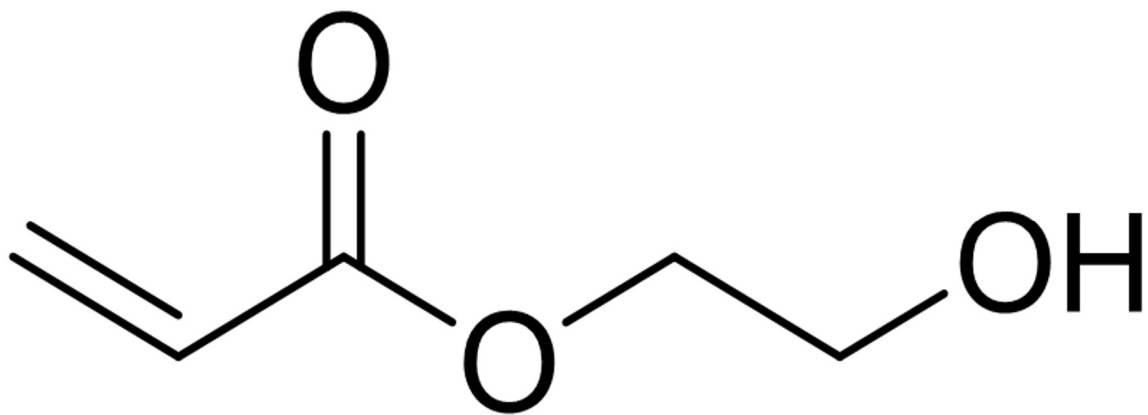


Figure 30: 2-HEA (CAS: 818-61-1)

2-HEA is used as a co-monomer in the manufacturing process of polymers and as a chemical reactant in the manufacturing of chemicals for further processing. Globally, nearly half of all 2-HEA produced is to assist in production of acrylic enamels for the automotive industry. 2-HEA finds numerous applications in automotive and architectural coatings, adhesives and more relevant to this thesis, photocurable resins.<sup>27</sup> Typical co-reactants include aromatic and aliphatic isocyanates, anhydrides and epoxides. With the acrylate functional group as a prime target for the photoinitiation, its place in the proposed mechanism in the introduction is illustrated below in Figure 31.

## 5.1.1.1 Occurrence in Photoinitiation

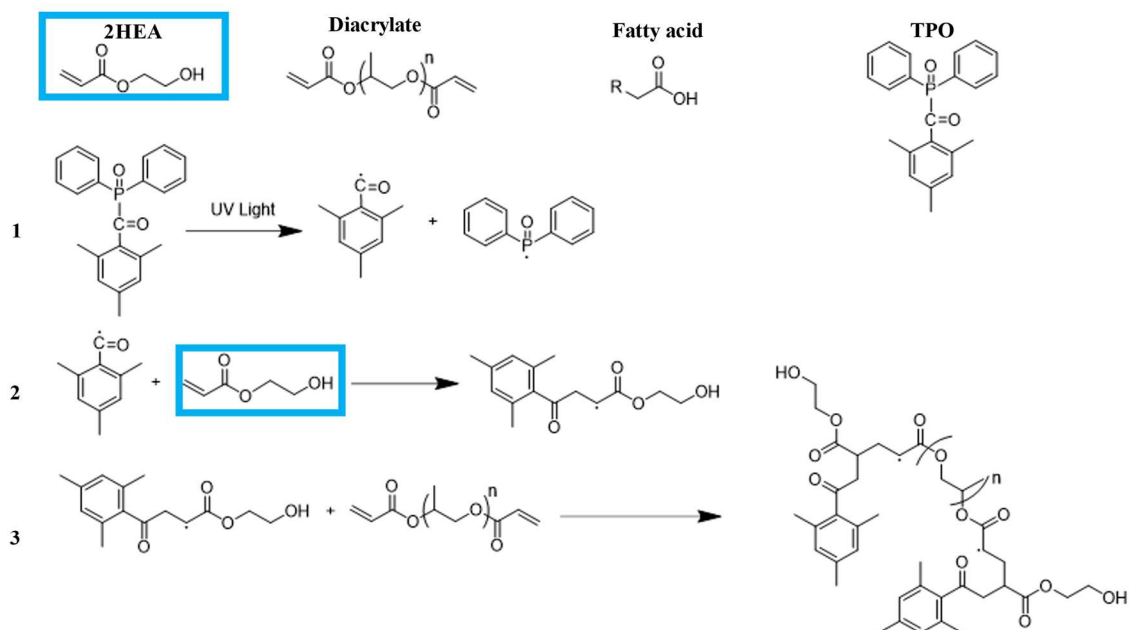


Figure 31: 2-HEA in the photopolymerization reaction.

The acrylate functional group makes this an ideal monomer for this polymerization reaction. When a radical interacts with the acrylate group, the propagation of radical chain polymerization begins.

## 5.1.1.2 Confirmation of Identity of 2-HEA by GC-MS

A mass spectrum from a purchased standard of 2-HEA (Figure 32) and a mass spectrum for the peak speculated to be 2-HEA in the SPME extract (Figure 33) are shown below.

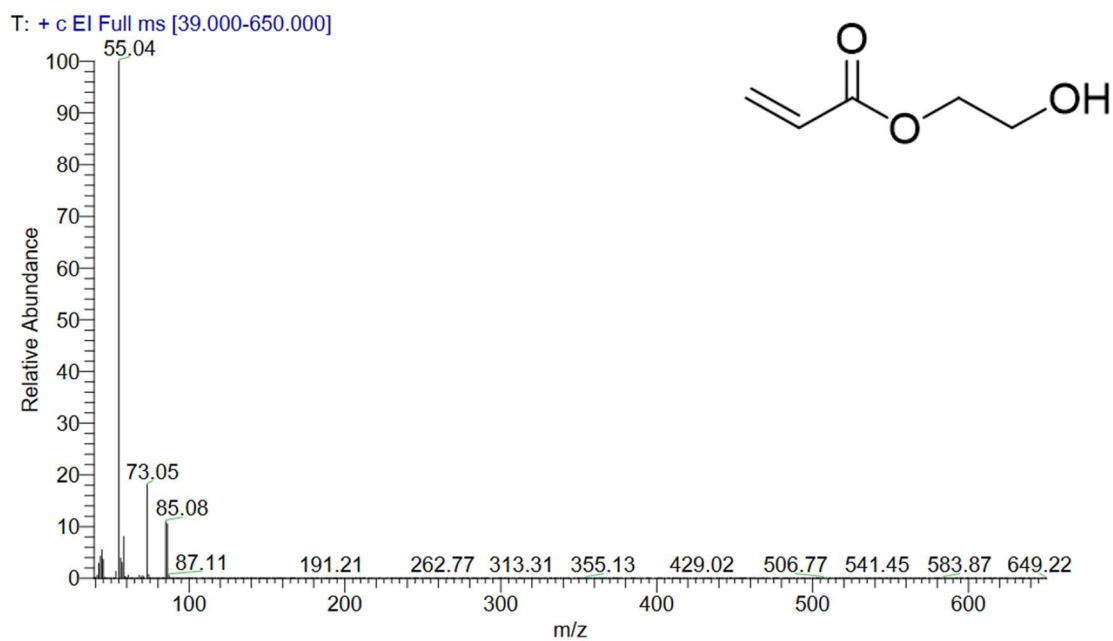


Figure 32: Mass spectrum of 2-HEA from purchased standard. (RT: 3.601)

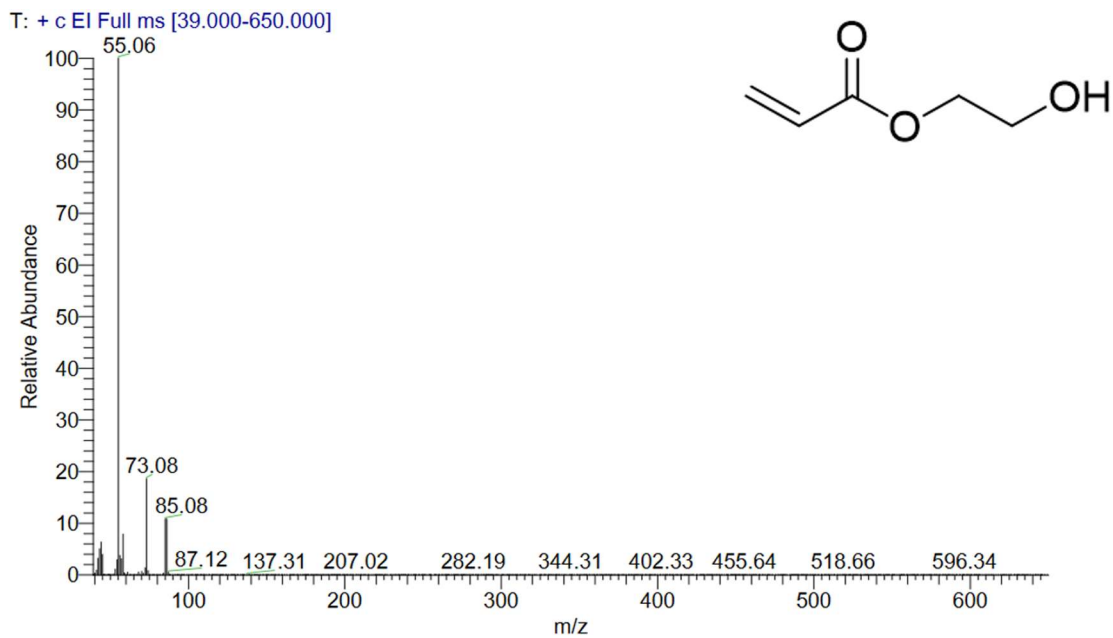


Figure 33: Mass spectrum of 2-HEA from resin experiment. (RT: 3.614)

Both spectra are dominated by peaks at  $m/z$  55, 73  $m/z$  and 85  $m/z$  in similar relative abundances. The molecular ion is not observed in either spectrum.

#### 5.1.2 4-Acryloylmorpholine (4-AM)

The structure of 4-AM is shown below in Figure 34.

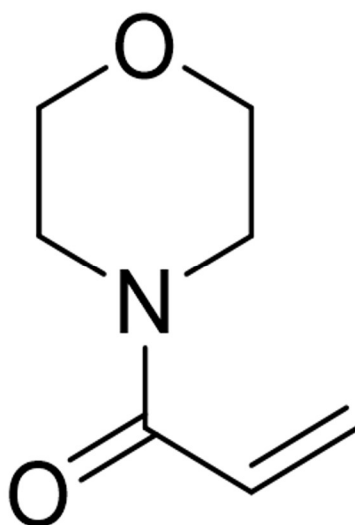


Figure 34: 4-AM structure.

4-AM has an acrylate group attached to a ring structure. The acrylate group puts 4-AM into the acrylate group as shown in Figure 3. <sup>7</sup> When a radical interacts with the acrylate group, the propagation of radical chain polymerization begins. The role of 4-AM in the photoinitiation is shown below in Figure 35.

##### 5.1.2.1 Occurrence in Photoinitiation

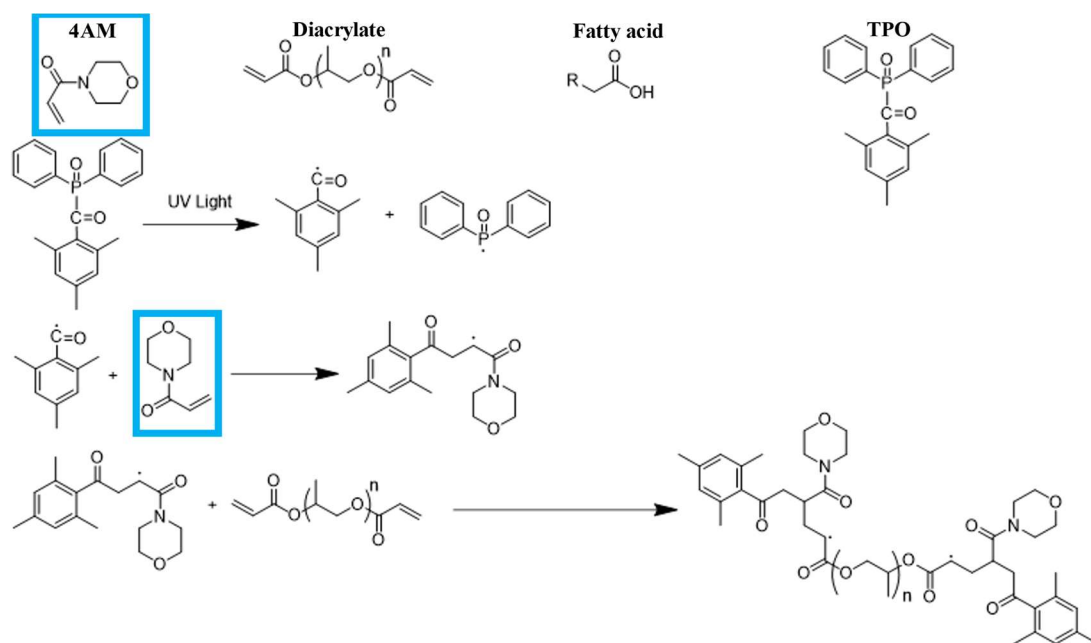


Figure 35: 4-AM in the photopolymerization reaction.

As with 2-HEA, 4-AM can be subjected to radical chain polymerization through interaction with a radical. This can happen not only with the photoinitiator fragment, but also with a radical containing 2-HEA. This mixed propagation adds diversity to the resin structure, and may even impart physical benefits such as rigidity and tensile strength to the final product.<sup>28</sup>

#### 5.1.2.2 Confirmation of Identity of 4-AM by GC-MS

A mass spectrum from a purchased standard of 4-AM (Figure 36) and a mass spectrum for the peak speculated to be 4-AM in the SPME extract (Figure 37) are shown below.

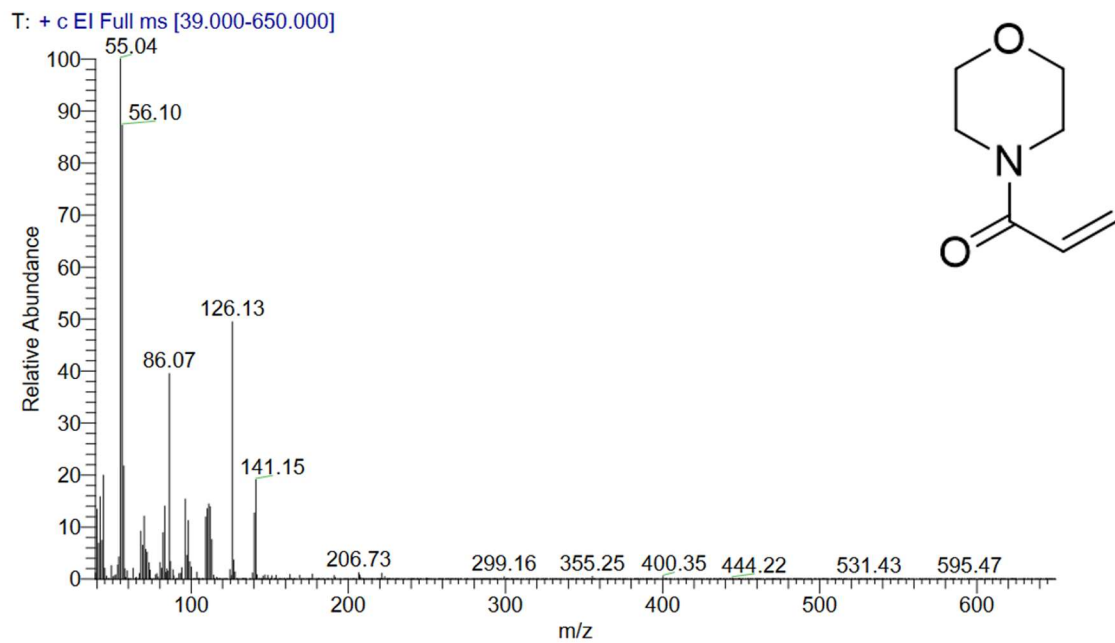


Figure 36: Mass spectrum of 4-AM from purchased standard. (RT: 6.102 min)

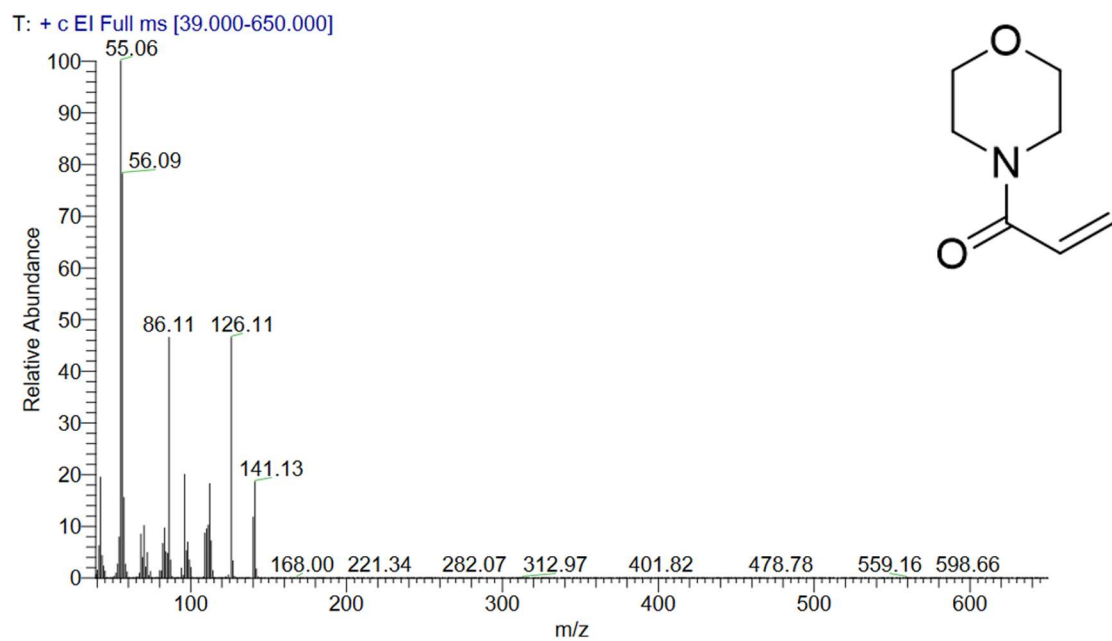


Figure 37: Mass spectrum of 4-AM from resin experiment. (RT: 6.020 min)

Both spectra are dominated by peaks at  $m/z$  55, 86  $m/z$  and 126  $m/z$  in similar relative abundances. The molecular ion is observed in both spectra at 141  $m/z$ .

### 5.1.3 Mesitaldehyde (MA)

The structure of MA is shown below in Figure 38.

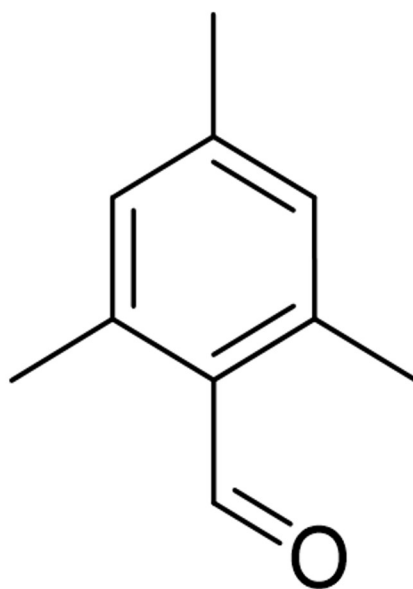


Figure 38: Structure of MA

MA has a benzene ring structure attached to an aldehyde functional group, and unlike the previously identified analytes, does not have an acrylate group. The absence of the acrylate prompted investigation into its involvement in other reported components of the photoinitiation reaction, specifically the photoinitiator. The compounds shown in Figure 39 are the two commonly used photoinitiators in resin manufacturing.<sup>7</sup>

#### 5.1.3.1 Occurrence in Photopolymerization



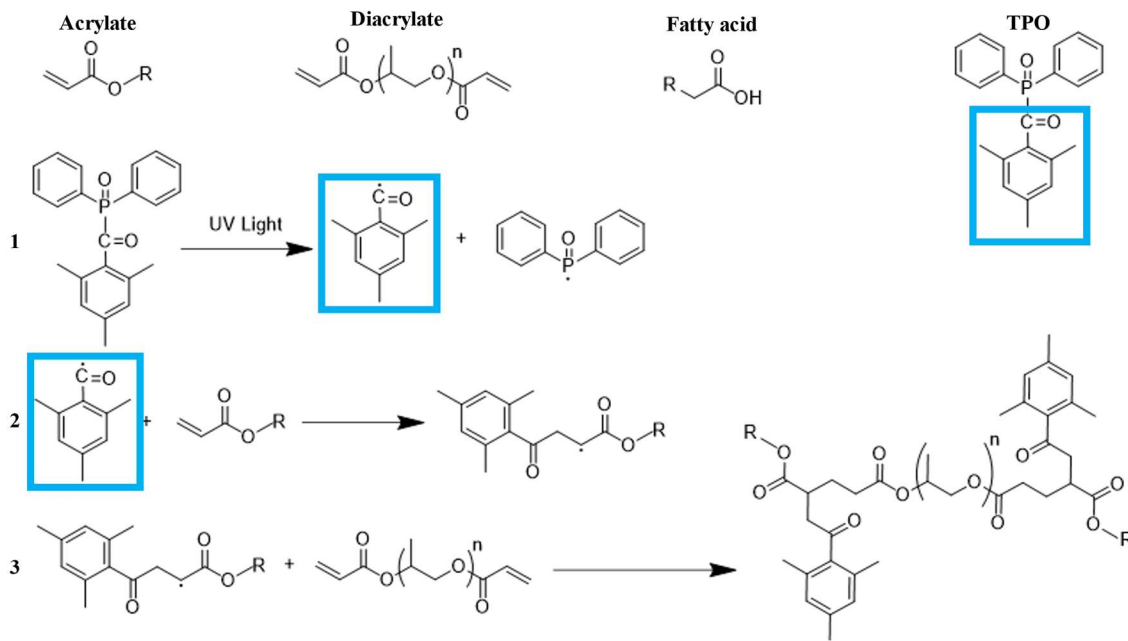


Figure 40: MA in the photopolymerization reaction.

As the photoinitiator is bombarded with UV light, the two new radicals are free to initiate the radical polymerization.

#### 5.1.3.2 Confirmation of Identity of MA by GC-MS

A mass spectrum from a purchased standard of MA (Figure 41) and a mass spectrum for the peak speculated to be MA in the SPME extract (Figure 42) are shown below.

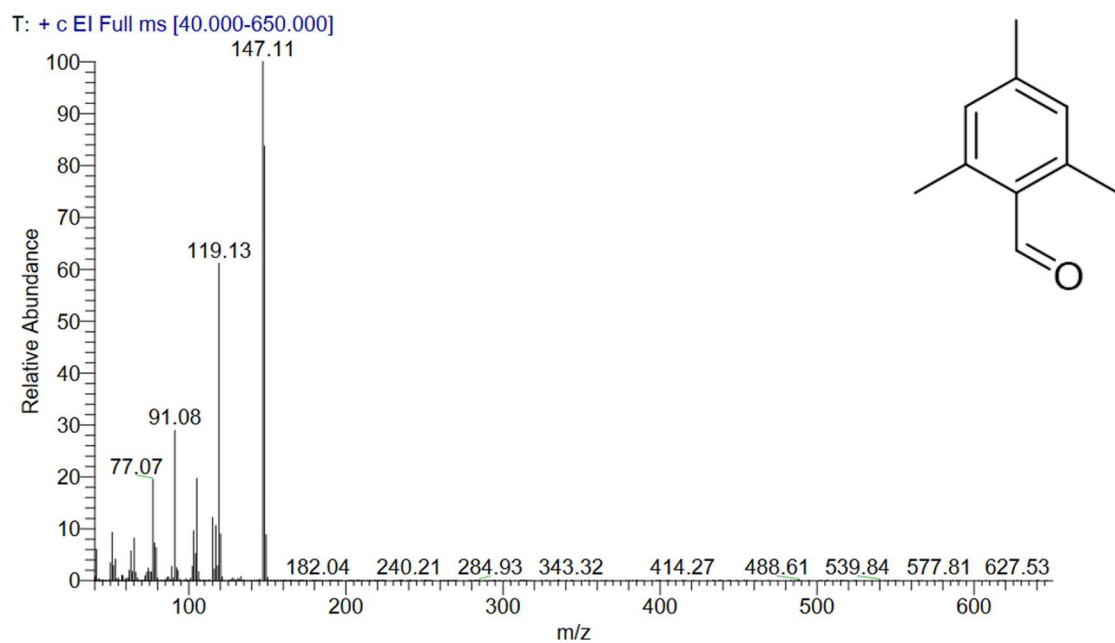


Figure 41: Mass spectrum of MA from purchased standard. (RT: 6.212 min)

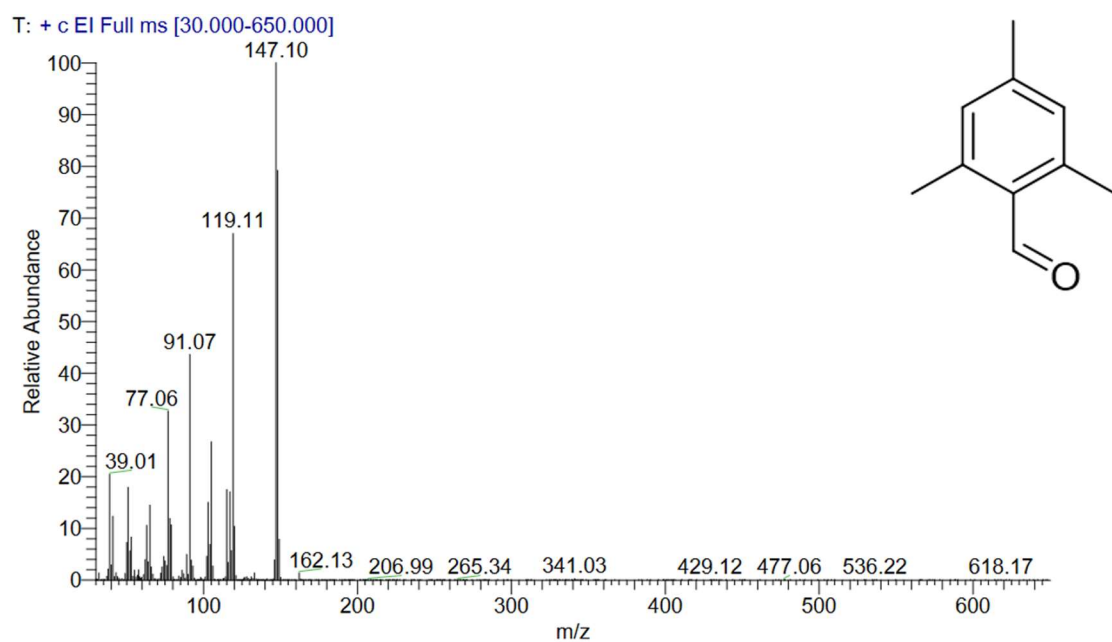


Figure 42: Mass spectrum of MA from resin experiment. (RT: 6.286 min)

Both spectra are dominated by peaks at  $m/z$  91, 119  $m/z$  and 147  $m/z$  in similar relative abundances.

#### 5.1.4 Toluene-2,4-diisocyanate (2,4-TDI)

The structure of 2,4-TDI is shown below in Figure 43.

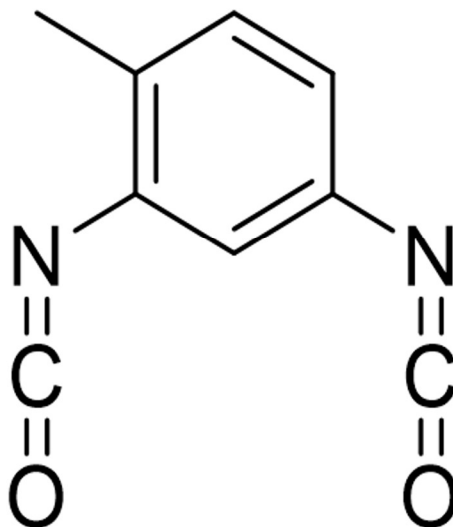


Figure 43: Structure of Toluene-2,4-diisocyanate.

2,4-TDI has a central benzene ring structure with a methyl group and two NCO functional groups in the 2 and 4 positions. It is commonly used as a chemical intermediate in the production of polyurethane foams and resin coatings.

#### 5.1.4.1 Occurrence in Photoinitiation

Diisocyanate compounds do not fall specifically into any of the established groups discussed, but potential uses can be theorized. In other applications, they are used as chain extenders, adding to the diversity of the polymer structure.<sup>28</sup> This is very similar to a crosslinker, that serves the same purpose with a similar functional group. If it is in fact a crosslinker, its involvement in the polymerization reaction could be depicted as in Figure 44.

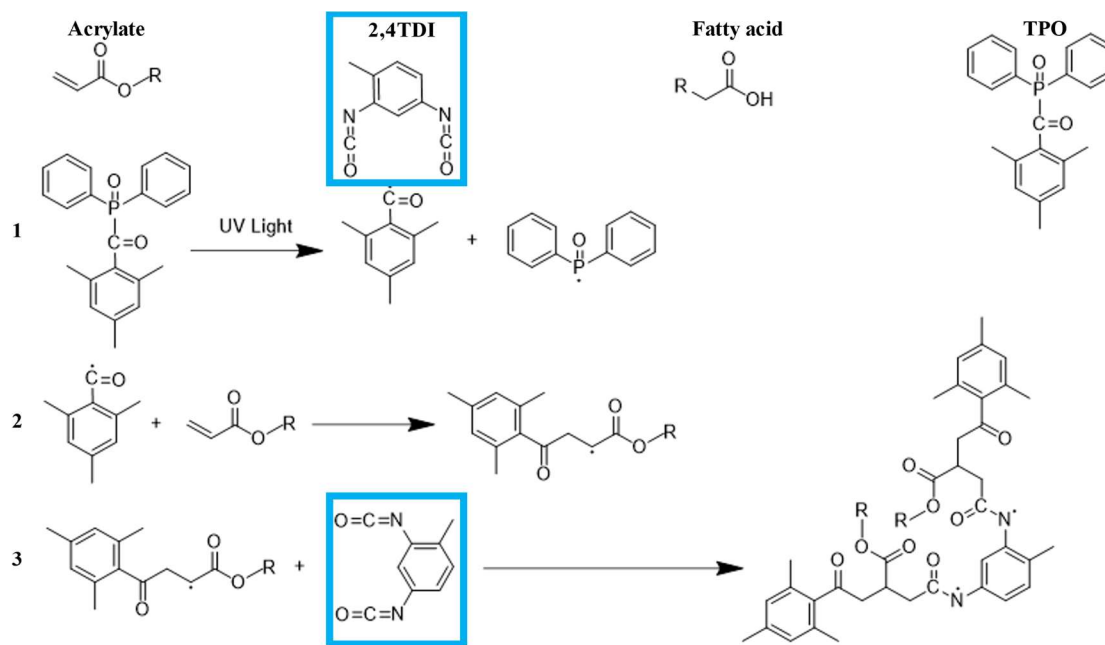


Figure 44: 2,4-TDI in the photopolymerization reaction.

#### 5.1.4.2 Confirmation of Identity of 2,4-TDI by GC-MS

A mass spectrum from a purchased standard of 2,4-TDI (Figure 45) and a mass spectrum for the peak speculated to be 2,4-TDI in the SPME extract (Figure 46) are shown below.

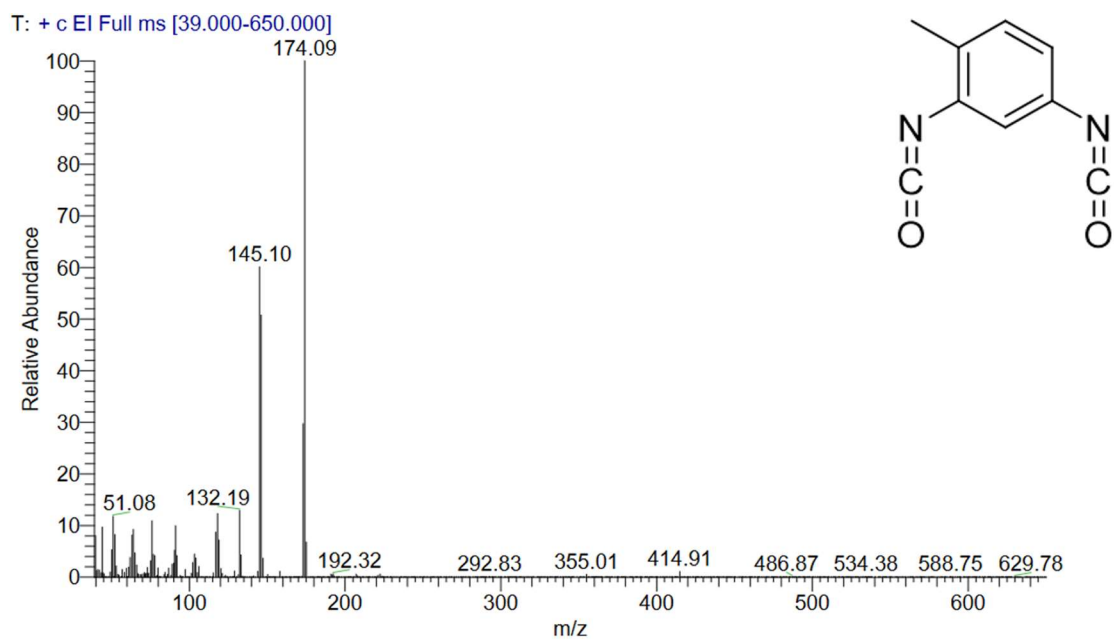


Figure 45: Mass spectrum for 2,4-TDI from purchased standard. (RT: 6.588 min)

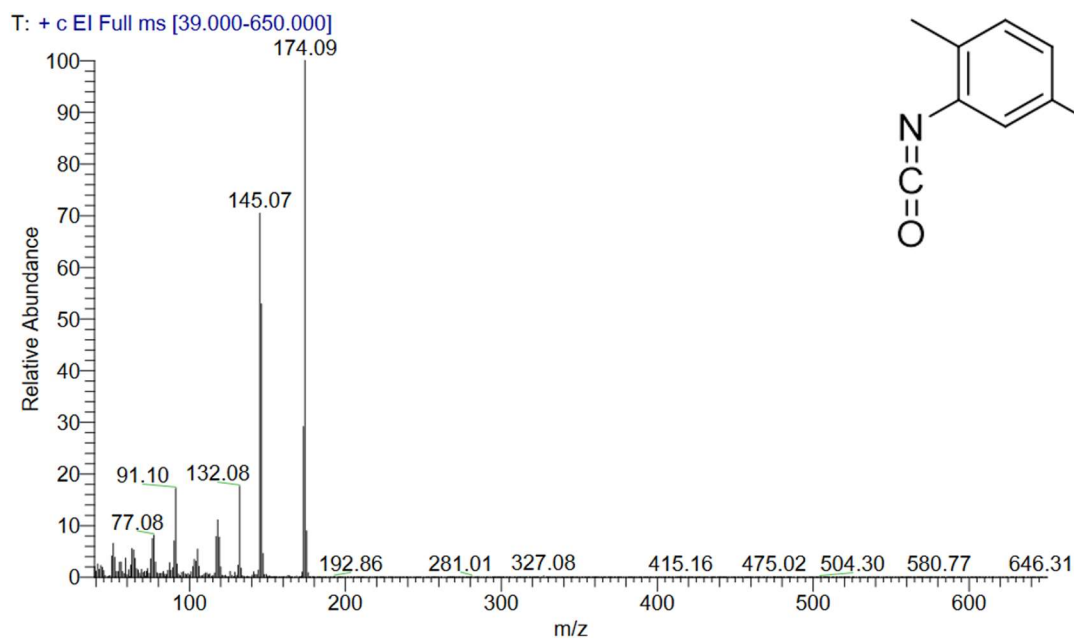


Figure 46: Mass spectrum for 2,4-TDI. (RT: 6.597 min)

Both spectra are dominated by peaks at 145 m/z and 174 m/z in similar relative abundances with the latter being the molecular ion.

#### 5.1.5 Dipropylene Glycol Diacrylate

The structure of Dipropylene Glycol Diacrylate (DPGDA) is shown below in Figure 47.

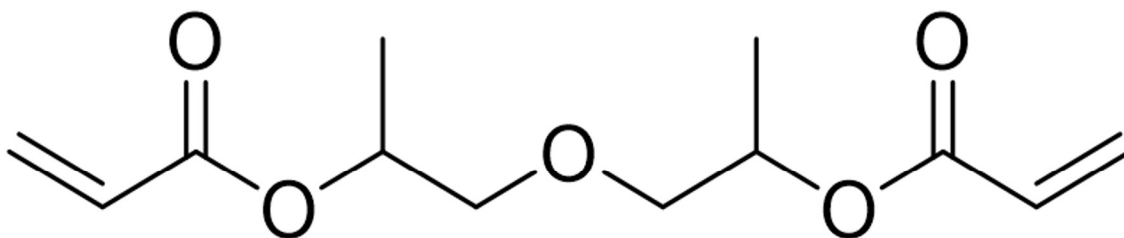


Figure 47: Structure of DPGDA.

DPGDA has a structure comprised of a propylene glycol chain with two terminal acrylate groups. This analyte can facilitate the photopolymerization at two different sites. This feature identifies DPGDA as a crosslinker as illustrated in Figure 48.

### 5.1.5.1 Occurrence in Photoinitiation

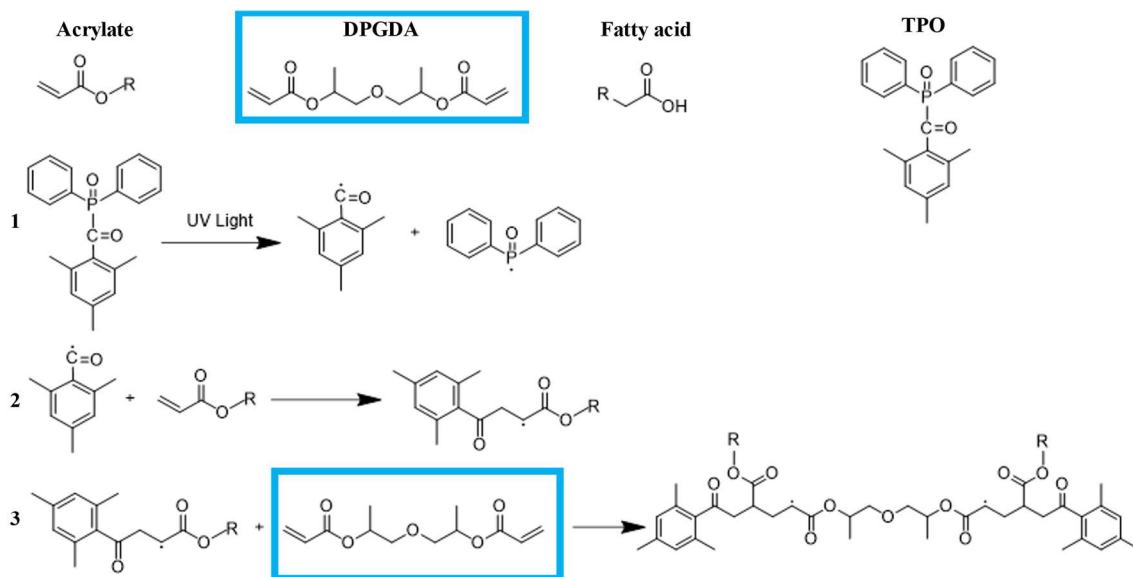


Figure 48: DPGDA in the photopolymerization reaction.

A crosslinker is used to expand the polymer chain in a second dimension, directly affecting the speed of photopolymerization.<sup>7,28</sup> With more sites for radical propagation, it happens at a faster rate.

### 5.1.5.2 Confirmation of Identity of DPGDA by GC-MS

A mass spectrum from a purchased standard of DPGDA (Figure 49) and a mass spectrum for the peak speculated to be DPGDA in the SPME extract (Figure 50) are shown below.

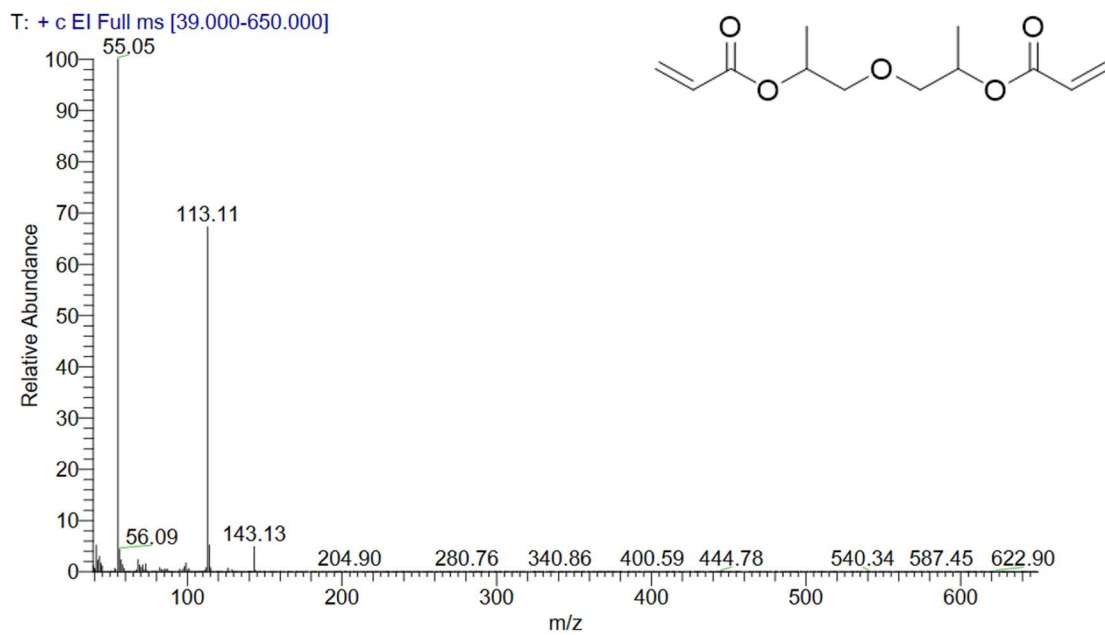


Figure 49: Mass spectrum of DPGDA from purchased standard. (RT: 7.350 min)

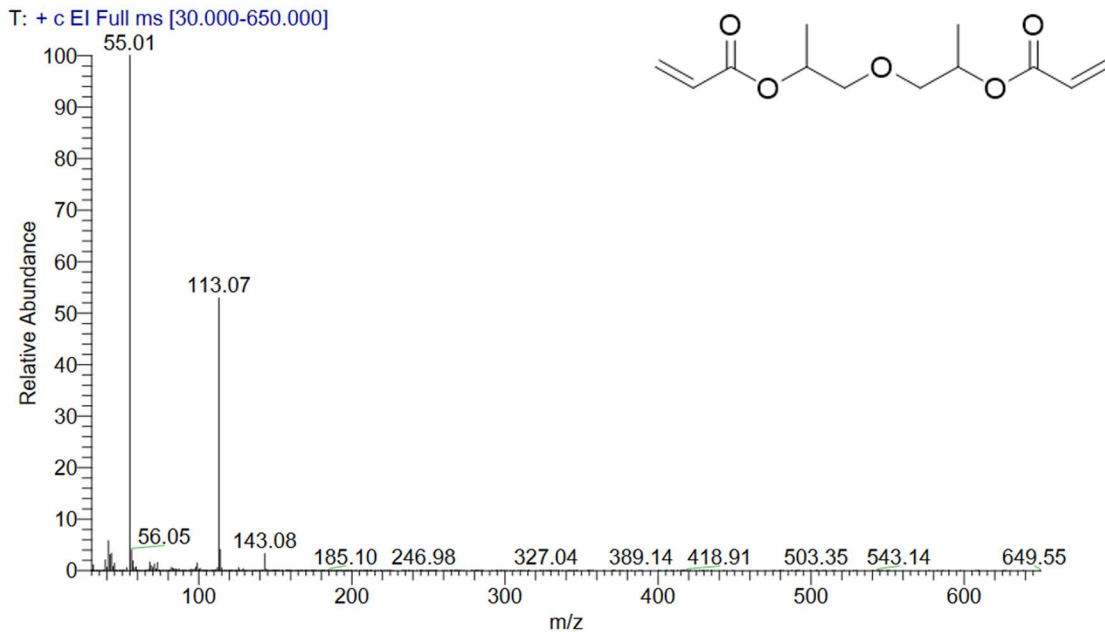


Figure 50: Mass spectrum of DPGDA from resin experiment. (RT: 7.363 min)

Both spectra are dominated by peaks at 55 m/z and 113 m/z in similar relative abundances.

#### 5.1.6 2,6-Di-Tert-Butyl-P-Cresol (BHT)

The structure of BHT is shown below in Figure 51.

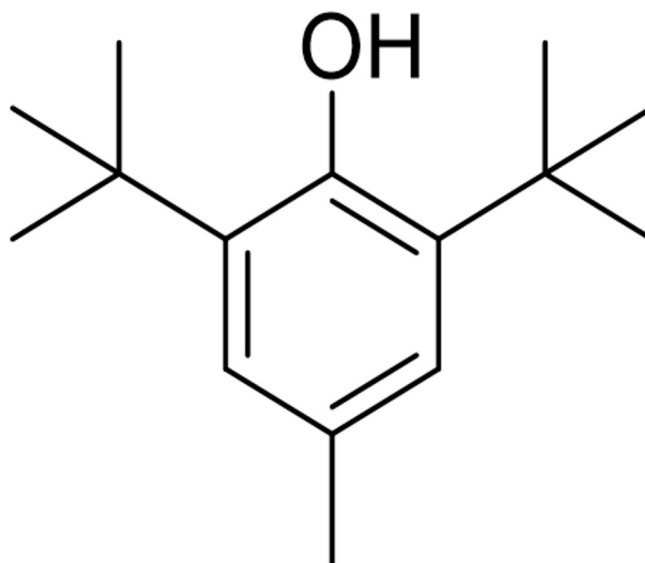


Figure 51: Structure of BHT.

BHT is a benzene ring with two tertbutyl groups, an OH group and a methyl attached.

##### 5.1.6.1 Occurrence in Photoinitiation

Unlike the other identified compounds, BHT is not directly involved in the polymerization. It is included in the mixture as a stabilizer to increase the shelf life of the liquid polymer.<sup>29</sup>

### 5.1.6.2 Confirmation of Identity of BHT by GC-MS

A mass spectrum from a purchased standard of BHT (Figure 52) and a mass spectrum for the peak speculated to be BHT in the SPME extract (Figure 53) are shown below.

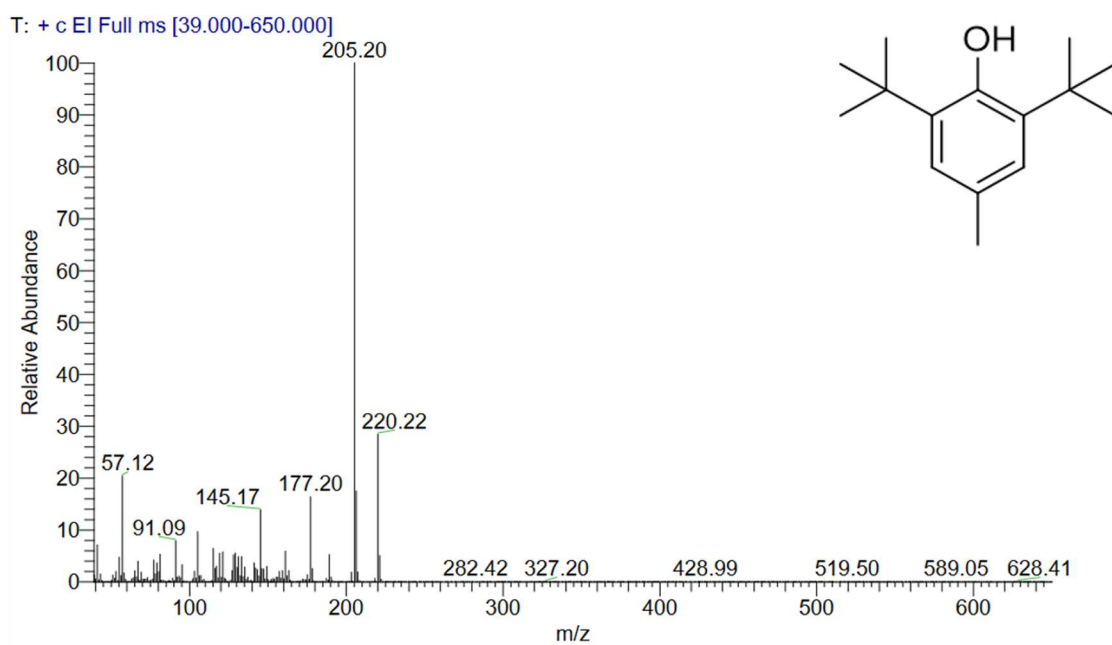


Figure 52: Mass spectrum of BHT from purchased standard. (RT: 7.521 min)

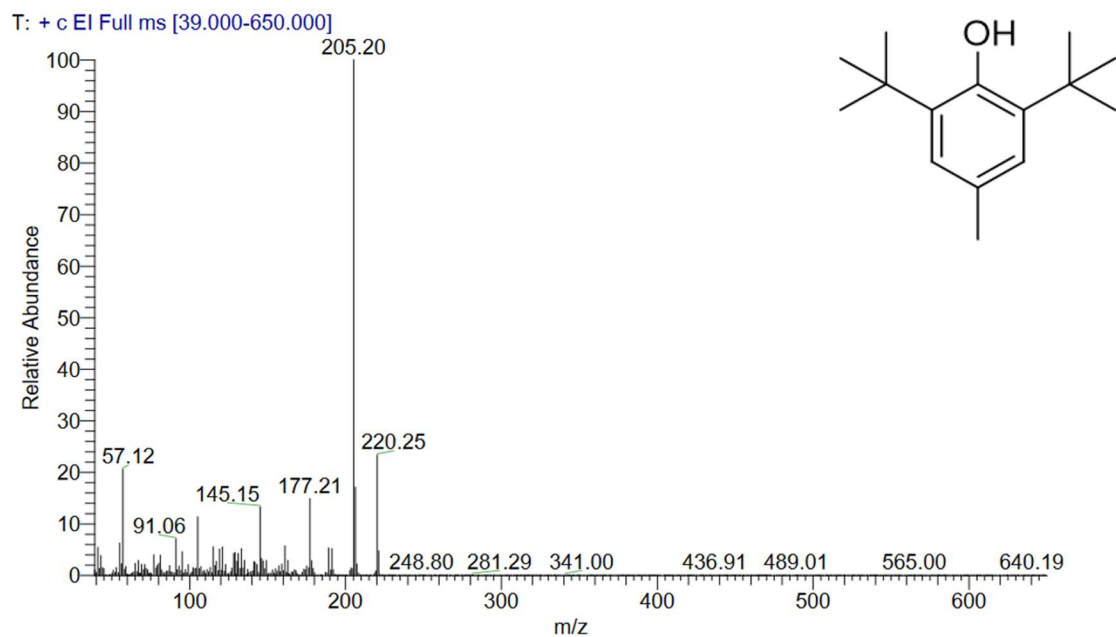


Figure 53: Mass spectrum of BHT from resin experiment. (RT: 7.574 min)

Both spectra are dominated by peaks at  $m/z$  205 and 220  $m/z$  in similar relative abundances with the latter being the molecular ion.

## 6 QUANTIFICATION

### 6.1 BLANKS

The experimental set up involved the measurement of each printing phase using the same enclosure. To investigate the possibility of carry over between phases, various blanks were analyzed, with the results shown in in the figures below. To ensure the absence of contamination in the enclosure itself, enclosure blanks were performed between phases. After the pre-phase experiment, the printer was removed completely from the enclosure and ambient air was pulled through the sampling system for 30 minutes. The enclosure was resealed and an experiment without a primary emission source was conducted. Figure 54 shows a chromatogram of the result of this enclosure blank experiment performed between the pre and during phases.

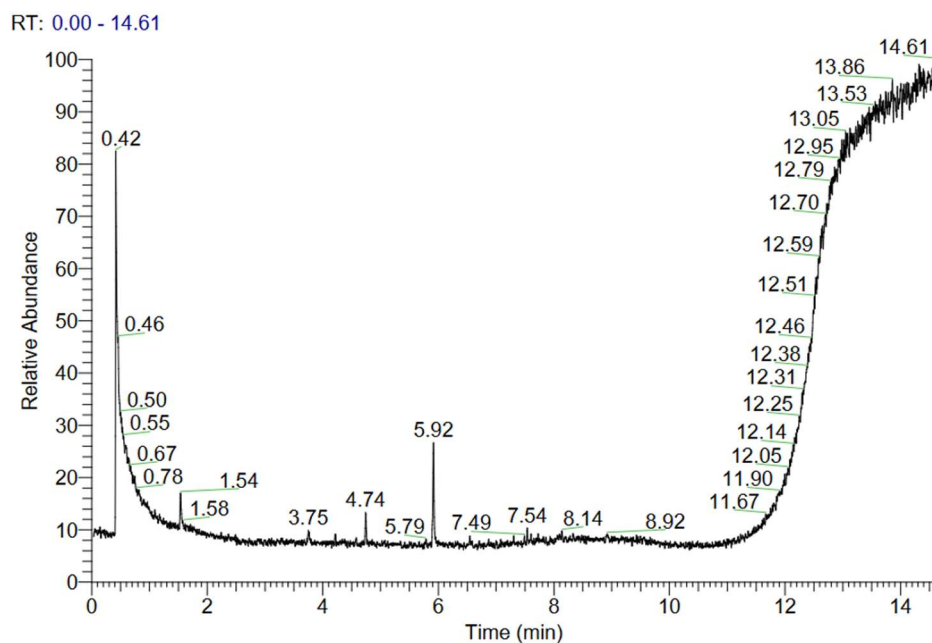
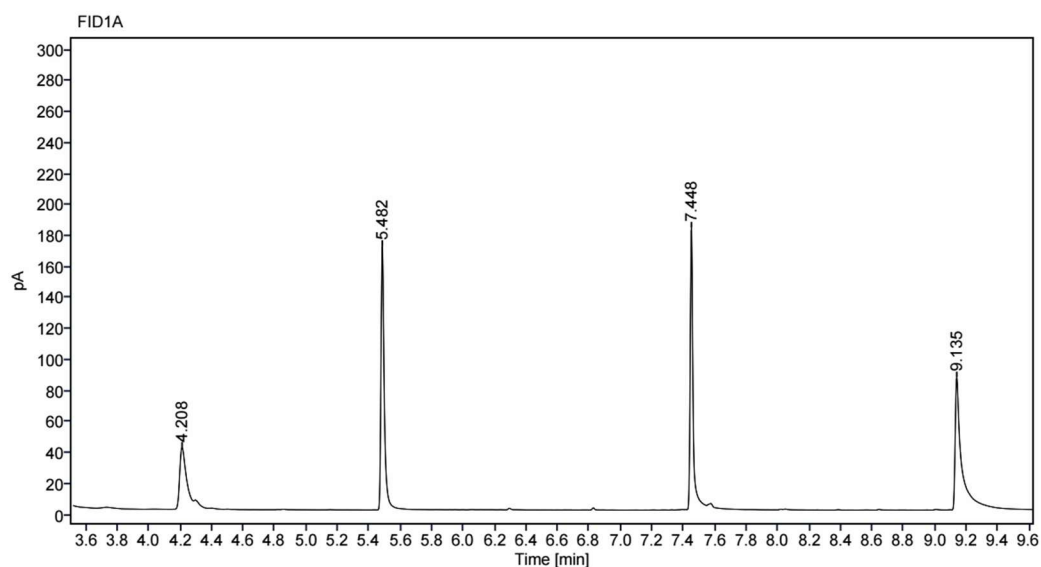


Figure 54: Enclosure Blank, taken between pre and during phases. Note that the peak at 5.92 min does not overlap with any of the six analytes measured.

Figure 55 shows a method blank. The experiment was performed without a printer or a post processing instrument inside. The PUF was extracted as per the procedure presented in the experimental section of this thesis, with the internal standard added and analyzed as a sample. This was done to ensure that the sample processing was not introducing any contamination or interfering peaks.



**Figure 55: Method blank. All four peaks correspond to the internal standard.**

Figure 56 shows an instrument blank for the GC-FID analysis method used for quantification with a solvent (dichloromethane) injection. This was done to ensure that the instrument itself did not introduce any contaminants or interfering peaks.

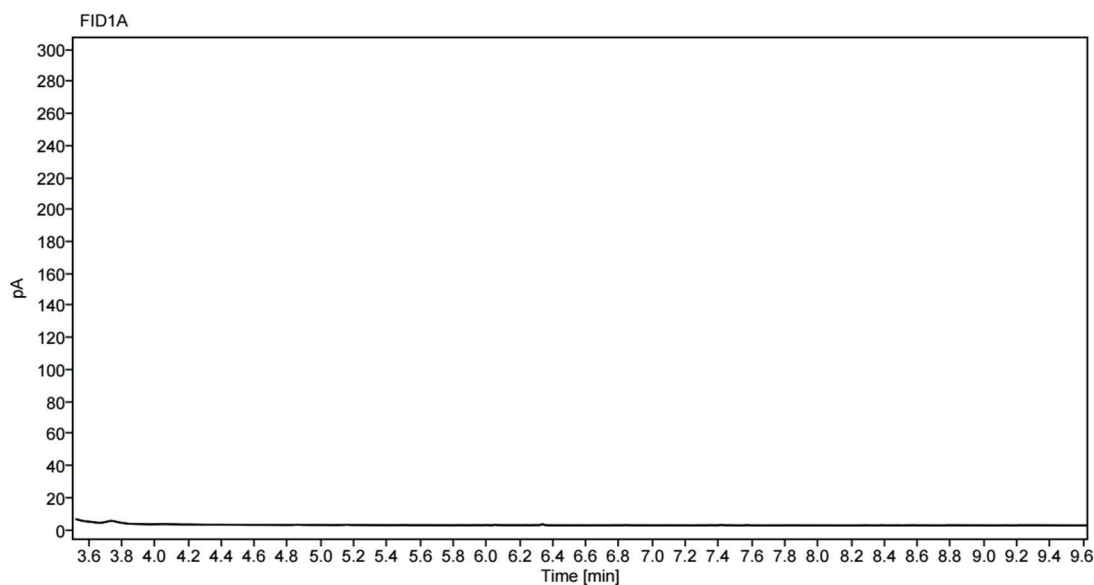


Figure 56: Instrument blank.

## 6.2 RECOVERY EXPERIMENTS

The experiment shown in Figure 28 was utilized to determine the recoveries at each level by dividing the observed concentration at each dilution level by the expected concentrations. The results are shown in Table 10 below.

Table 8: Average recovery percentages for each analyte across all three levels of concentration. Standard deviation in parenthesis.

Dilution Level	2-HEA	4-AM	MA	2,4-TDI	DPGDA	BHT
[U]	85 (6)	87 (9)	83 (7)	80 (11)	85 (11)	80 (11)
[1000]	81 (3)	75 (5)	72 (4)	67 (9)	74 (4)	66 (4)
[200]	51 (1)	48 (1)	48 (3)	49 (8)	51 (4)	39 (4)

There is an observed correlation between post sample processing concentration and low recovery for all six analytes. This can be explained by the nature of the concentrating samples via rapid evaporation. By volatilizing the analyte loaded solvent, the different compounds of interest are also volatilized and lost. Though not ideal, it was necessary to concentrate samples to bring some of the less abundant analytes above the LOD. All quantification results will indicate which concentration level the data was gathered from so the associated recoveries can be considered.

### 6.3 CONCENTRATION OF SIX VOCs IN OIL-BASED RESIN

Using the processing methods and GC-FID analysis outlined in the experimental section above, the concentrations of the six identified VOCs in the emissions of each printing phase were determined for the oil-based feedstock. The results are shown below in Figures 57-62. The concentrations, reported in micrograms of analyte per gram of resin printed, are reported in Table 9. As shown, the concentrations are lowest for BHT and highest for 4-AM.

**Table 9: Mean and standard deviation in concentrations of quantified analytes in oil-based printer emissions (n=4). All concentrations are reported in µg/g resin printed. Italicized values were generated in the highest amount of evaporative concentration, which show the largest methodological losses. (See Table 10)**

			<b>2-HEA</b>	<b>4-AM</b>	<b>MA</b>	<b>2,4-TDI</b>	<b>DPGDA</b>	<b>BHT</b>
<b>Detection Limit</b>			0.214	0.179	0.186	0.2543	0.242	0.0121
Cube	Pre	Mean	19.8	134	<i>0.71</i>	3.52	4.60	<i>0.132</i>
		SD	0.90	2.03	<i>0.127</i>	0.889	0.345	<i>0.006</i>
Cube	During	Mean	20.7	103	<i>0.870</i>	<i>0.460</i>	3.65	<i>0.161</i>
		SD	0.720	1.94	<i>0.160</i>	<i>0.078</i>	0.169	<i>0.014</i>
Cube	Wash	Mean	1.60	15.5	<i>0.734</i>	3.59	1.60	<i>0.139</i>
		SD	0.06	0.855	<i>0.123</i>	0.779	0.094	<i>0.006</i>
Cube	Cure	Mean	<i>0.56</i>	25.9	<i>0.803</i>	3.87	1.79	<i>0.152</i>
		SD	<i>0.08</i>	1.010	<i>0.136</i>	0.674	0.281	<i>0.008</i>
Square Pyramid	Pre	Mean	18.4	135	<i>0.660</i>	3.30	4.09	<i>0.126</i>
		SD	0.98	3.09	<i>0.123</i>	0.805	0.189	<i>0.008</i>
Square Pyramid	During	Mean	20.7	103	<i>0.884</i>	<i>0.606</i>	3.82	<i>0.173</i>
		SD	1.200	2.49	<i>0.166</i>	<i>0.223</i>	0.260	<i>0.017</i>
Square Pyramid	Wash	Mean	2.52	15.2	<i>0.621</i>	4.59	2.12	<i>0.124</i>
		SD	0.477	0.727	<i>0.105</i>	0.920	0.195	<i>0.006</i>
Square Pyramid	Cure	Mean	<i>0.523</i>	26.3	<i>0.691</i>	4.20	1.98	<i>0.141</i>
		SD	<i>0.032</i>	0.955	<i>0.117</i>	0.915	0.307	<i>0.009</i>

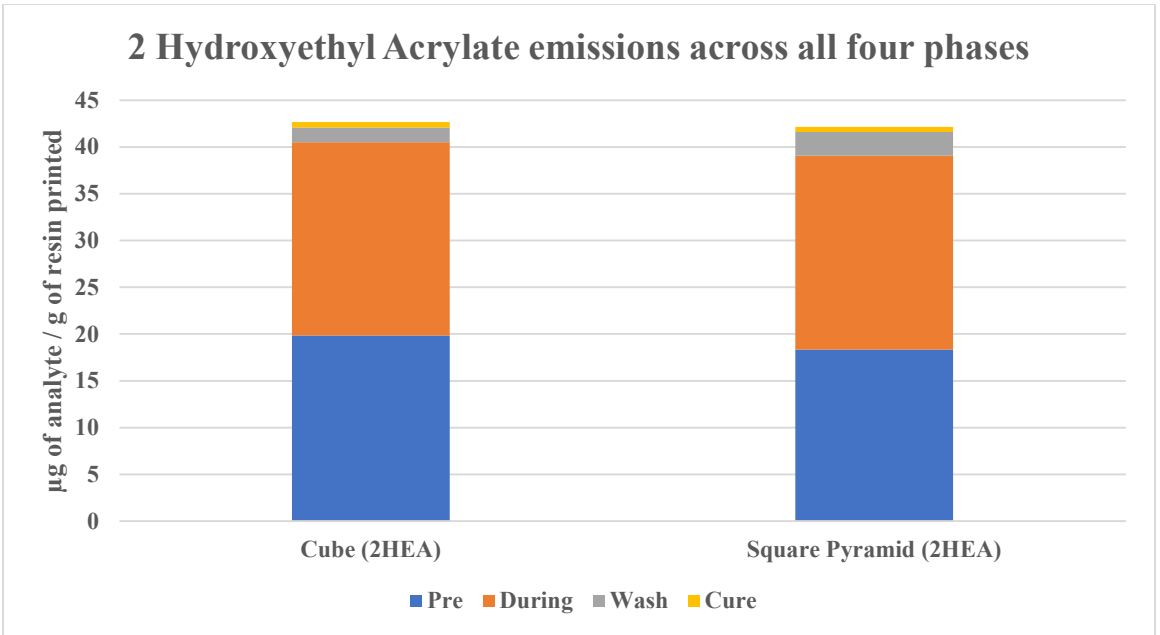


Figure 57: 2-HEA emissions across all four phases.

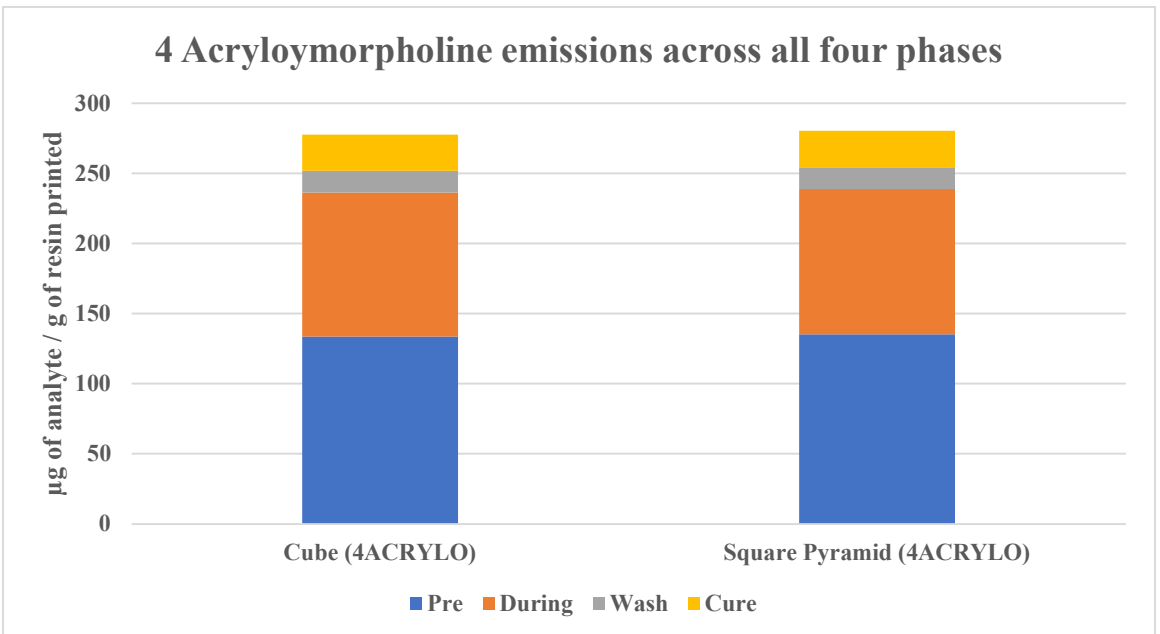


Figure 58: 4-AM emissions across all four phases.

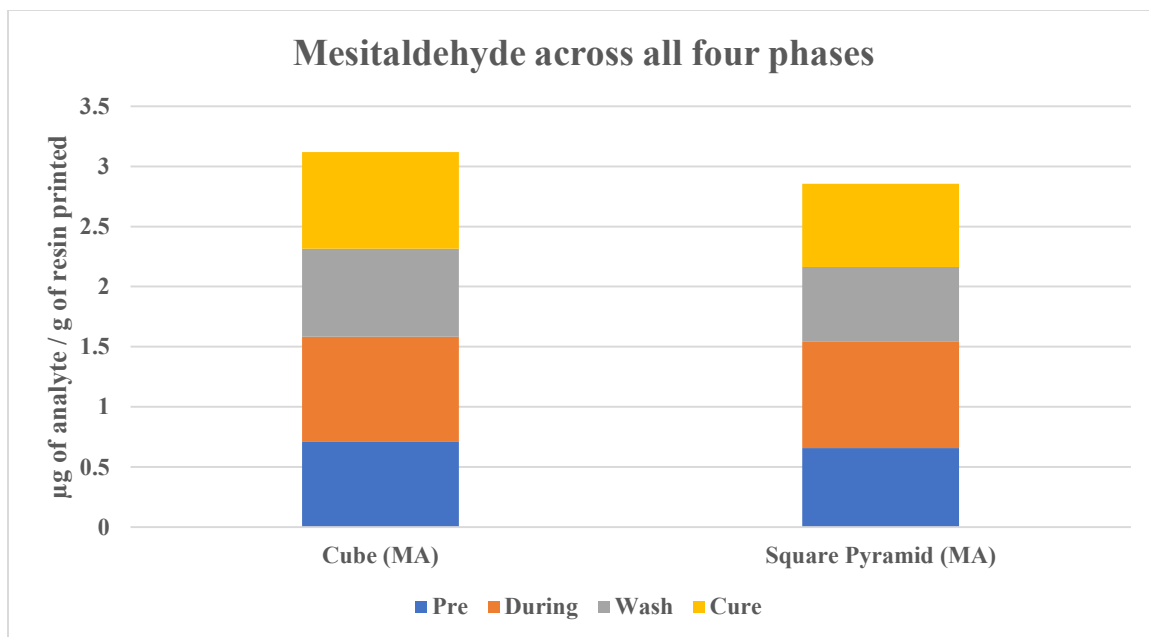


Figure 59: MA emissions across all four phases.

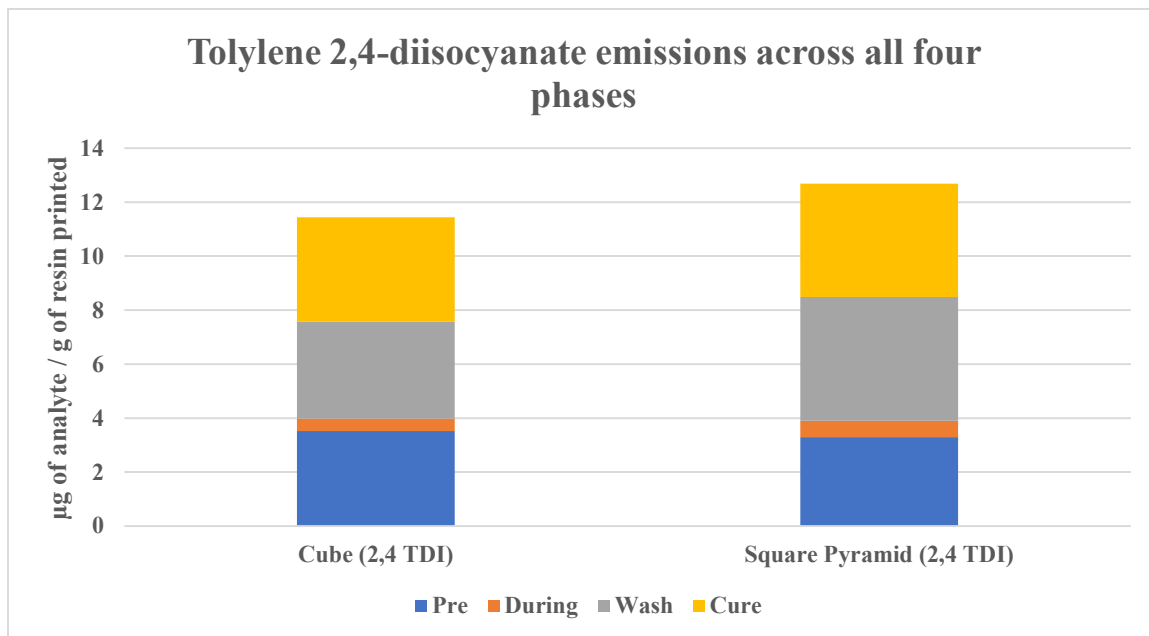


Figure 60: 2,4-TDI emissions across all four phases.

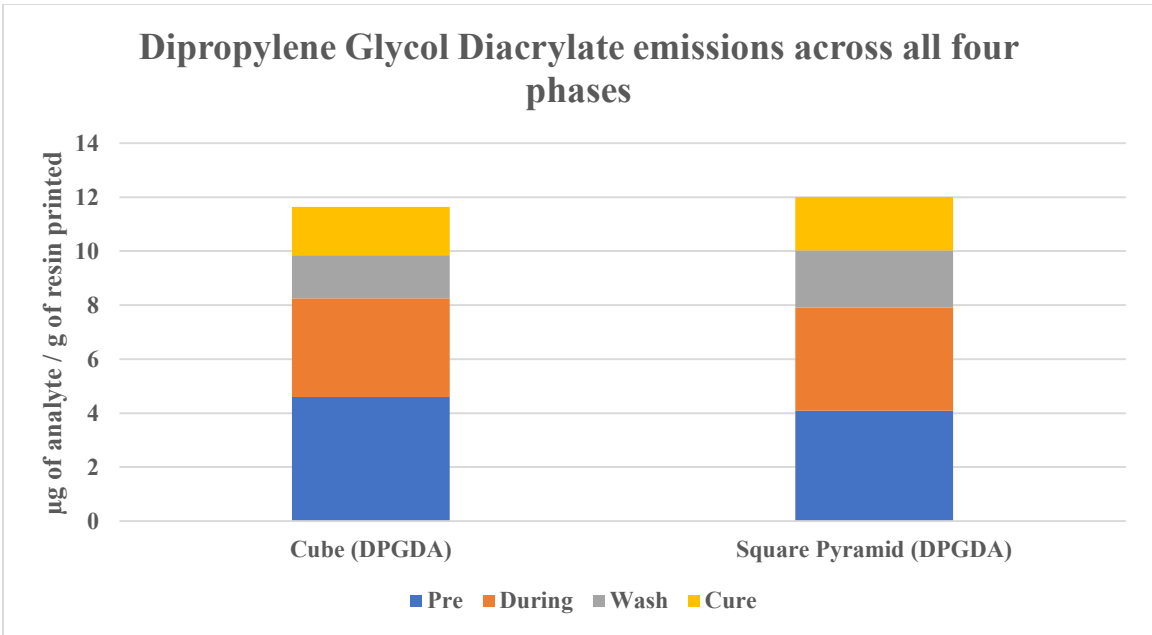


Figure 61: DPGDA emissions across all four phases.

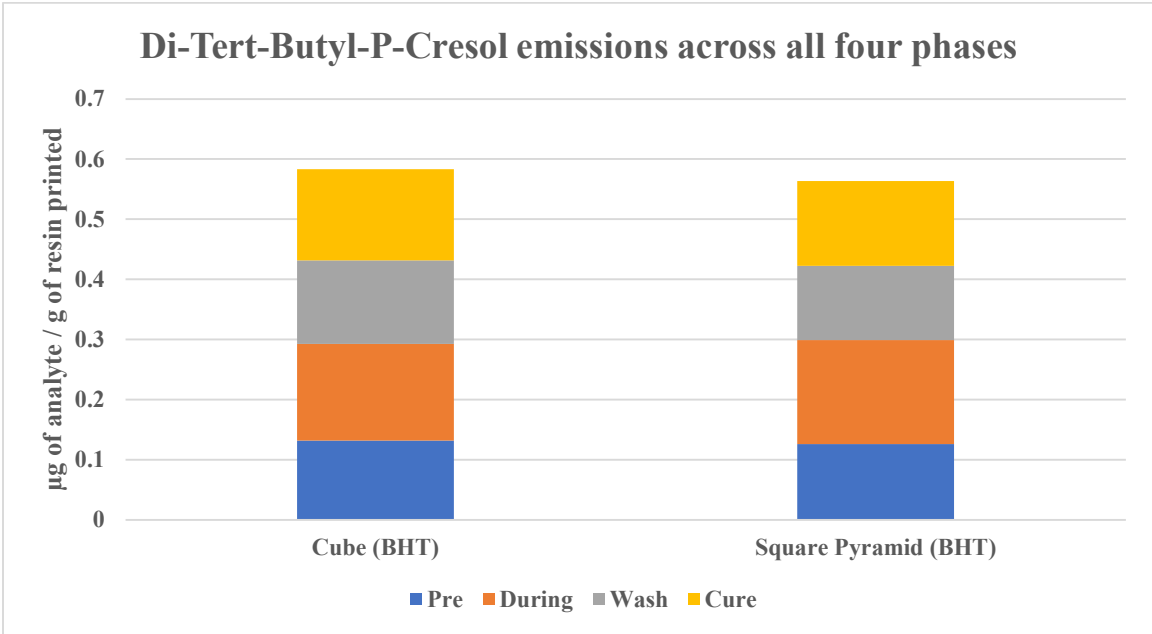


Figure 62: BHT emissions across all four phases.

4-AM was the only analyte detectable across all phases in the unconcentrated concentration level. The pre phase when the printer is idle, showed 4-AM in an amount of 133.58  $\mu\text{g}$  per gram of resin printed. BHT had the lowest emission in the wash phase, at 0.12  $\mu\text{g}$  per gram of resin printed. A key observation from the data above is the similarity in overall emission (total emission) and emissions in each phase between the two printed shapes. The results are well within the standard deviation of the measurements, and so the analyte concentrations were averaged between the shapes to generate a single set of emissions data for Figure 63. Figure 64 omits 2-HEA and 4-AM to better present the other four analytes.

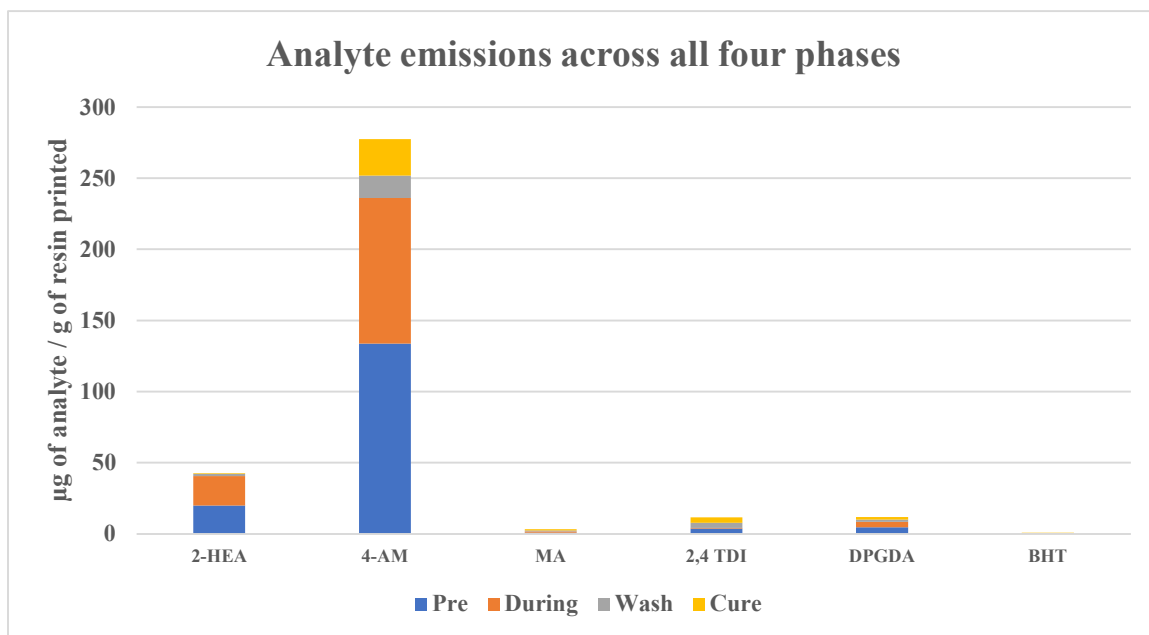
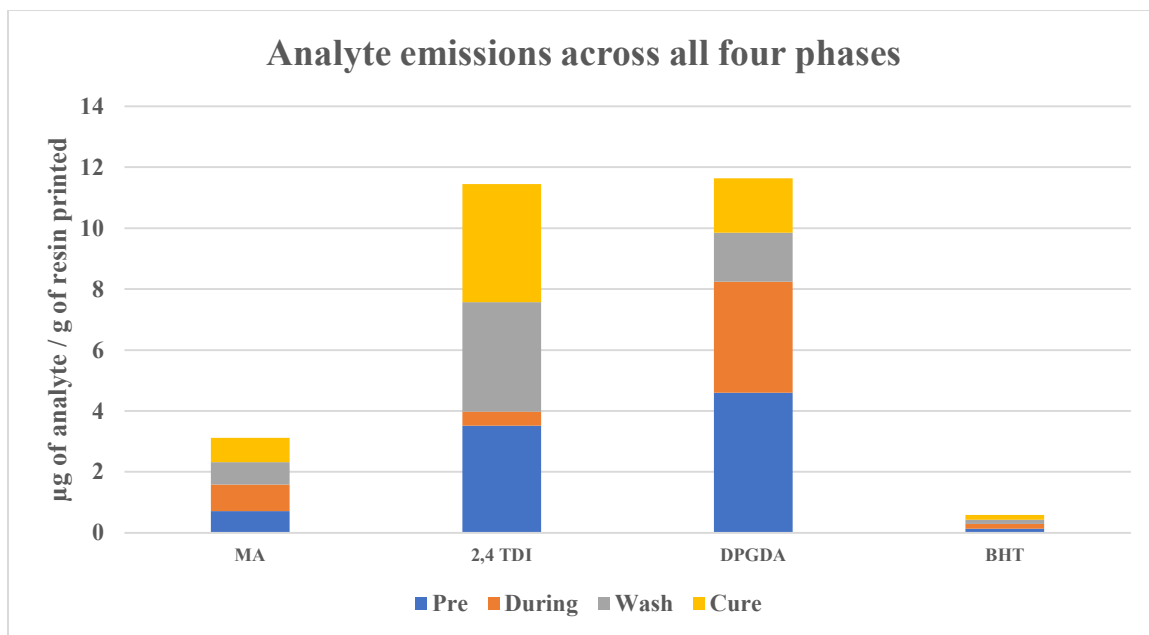


Figure 63: Emissions across all phases for all 6 analytes. (Oil-based resin)



**Figure 64: Emissions across all phases for 4 analytes using the oil-based resin. (2-HEA and 4-AM omitted to emphasize the other four analytes.)**

#### 6.4 CONCENTRATION OF SIX VOCs IN PLANT-BASED RESIN

All of the experiments for the oil-based resin were replicated with plant-based resin to investigate the possibility of a markable reduction in emission. Using the processing methods and GC-FID analysis outlined in the experimental section above, the concentrations of the six identified VOCs in the emissions of each printing phase were determined for the plant-based feedstock. The results are shown below in Figures 65-70. These concentrations, reported in micrograms of analyte per gram of resin printed, are reported in Table 10. Similar to the oil-based analysis the concentrations are lowest for BHT and highest for 4-AM.

**Table 10: Mean and standard deviation in concentrations of quantified analytes in plant-based printer emissions (n=4). All concentrations are reported in µg/g resin printed. Italicized values were generated in the highest amount of evaporative concentration, which show the highest amount of methodological loss. (See Table 10)**

			<b>2-HEA</b>	<b>4-AM</b>	<b>MA</b>	<b>2,4-TDI</b>	<b>DPGDA</b>	<b>BHT</b>
Detection Limit			0.214	0.179	0.186	0.2543	0.242	<i>0.0121</i>
Cube	Pre	Mean	8.92	50.6	<i>1.15</i>	1.46	2.06	<i>0.201</i>
		SD	1.10	5.36	<i>0.176</i>	0.198	0.276	<i>0.029</i>
Cube	During	Mean	13.0	55.4	<i>0.893</i>	<i>0.261</i>	1.83	<i>0.225</i>
		SD	0.283	6.95	<i>0.189</i>	<i>0.034</i>	0.080	<i>0.019</i>
Cube	Wash	Mean	<i>0.844</i>	8.02	<i>0.567</i>	1.26	<i>0.804</i>	<i>0.030</i>
		SD	<i>0.02</i>	0.280	<i>0.063</i>	0.114	<i>0.146</i>	<i>0.002</i>
Cube	Cure	Mean	<i>0.24</i>	11.2	<i>0.656</i>	1.57	<i>0.852</i>	<i>0.030</i>
		SD	<i>0.00</i>	0.990	<i>0.079</i>	0.262	<i>0.109</i>	<i>0.004</i>
Sq Pyr	Pre	Mean	9.32	50.2	<i>1.18</i>	1.41	1.78	<i>0.228</i>
		SD	0.30	1.08	<i>0.304</i>	0.143	0.158	<i>0.027</i>
Sq Pyr	During	Mean	13.1	55.6	<i>0.772</i>	<i>0.245</i>	1.93	<i>0.213</i>
		SD	0.632	6.14	<i>0.059</i>	<i>0.045</i>	0.159	<i>0.022</i>
Sq Pyr	Wash	Mean	<i>0.846</i>	8.89	<i>0.666</i>	1.42	<i>0.823</i>	<i>0.032</i>
		SD	<i>0.092</i>	0.847	<i>0.075</i>	0.113	<i>0.143</i>	<i>0.002</i>
Sq Pyr	Cure	Mean	<LOD	8.28	<i>0.581</i>	1.43	<i>0.867</i>	<i>0.027</i>
		SD	<LOD	0.432	<i>0.059</i>	0.304	<i>0.073</i>	<i>0.002</i>

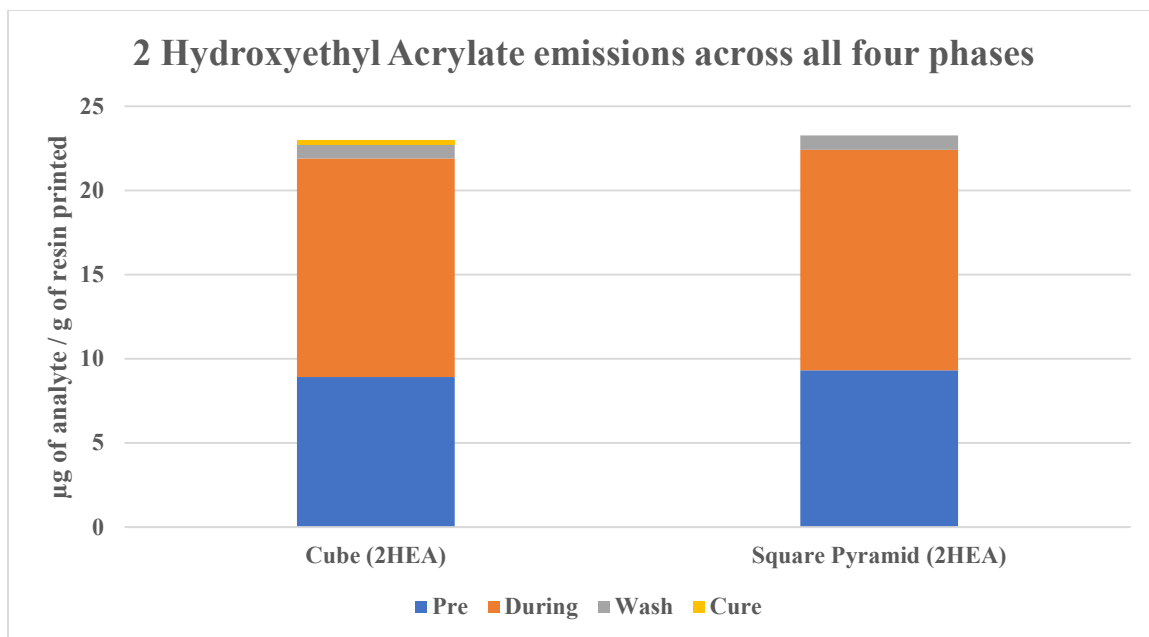


Figure 65: 2-HEA emissions across all four phases (Plant-based resin)

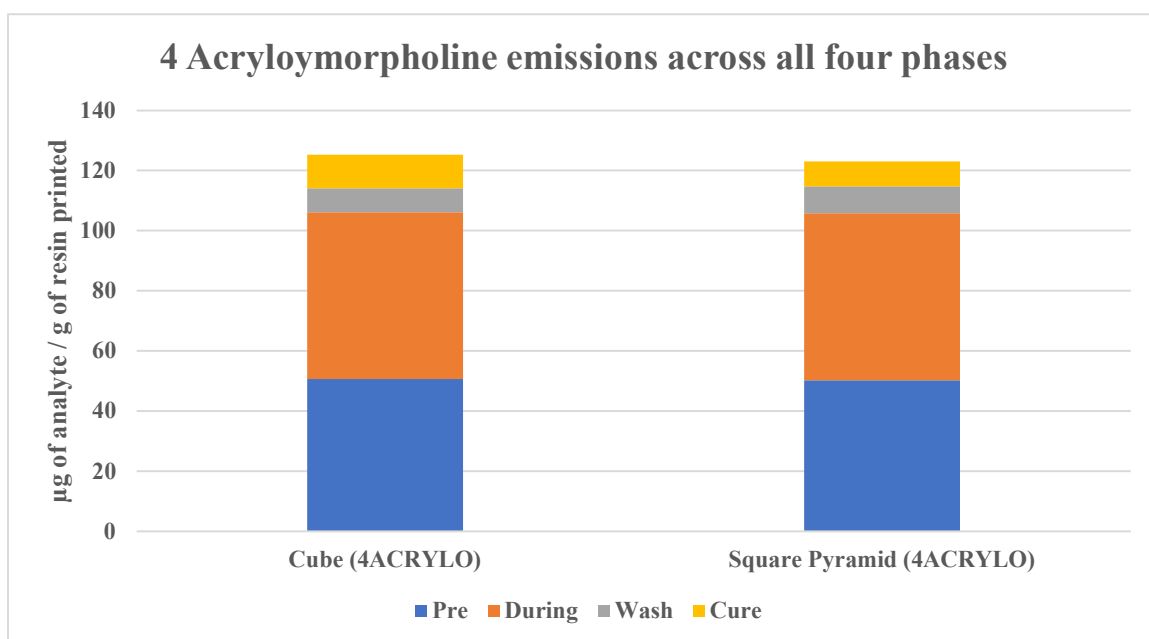


Figure 66: 4-AM emissions across all four phases. (Plant-based resin)

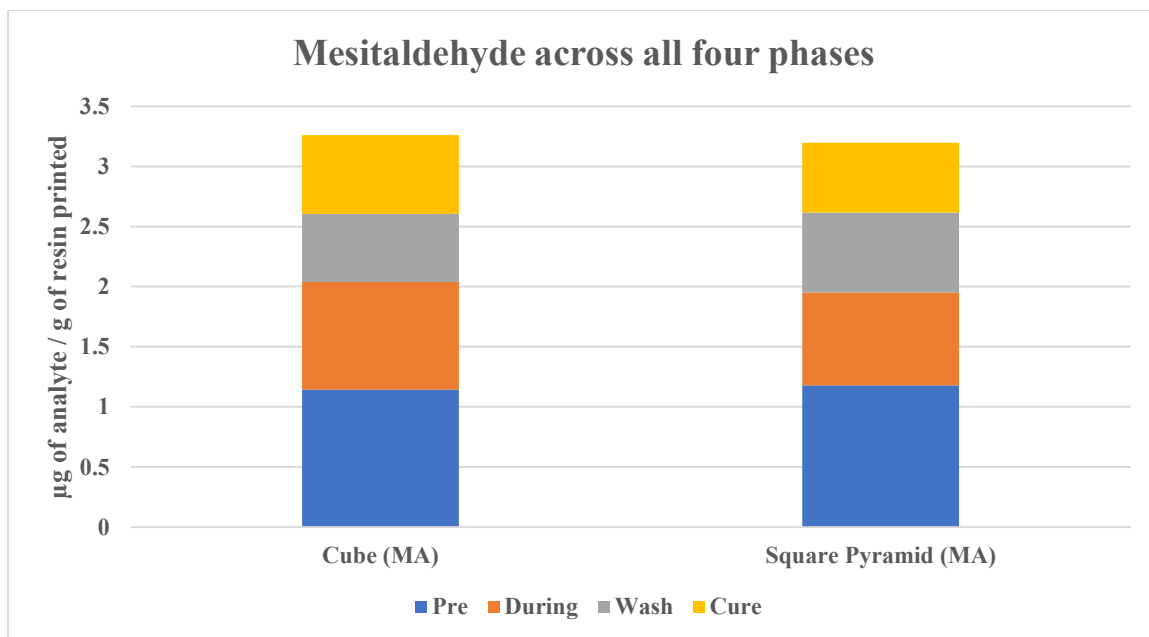


Figure 67: MA emissions across all four phases. (Plant-based resin)

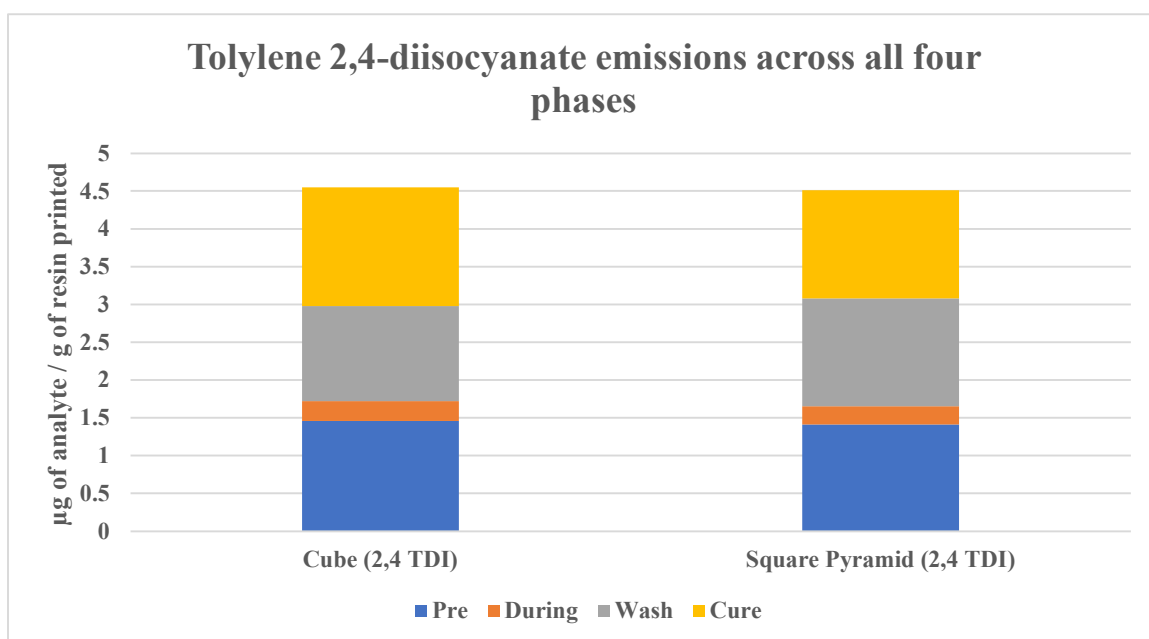


Figure 68: 2,4-TDI emissions across all four phases. (Plant-based resin)

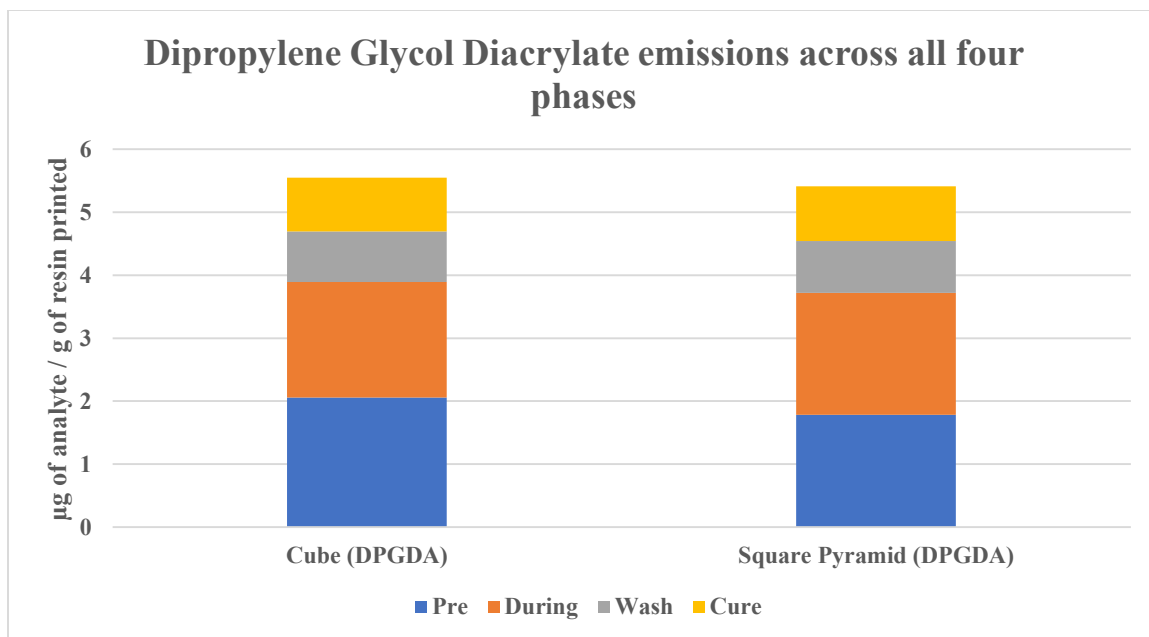


Figure 69: DPGDA emissions across all four phases. (Plant-based resin)

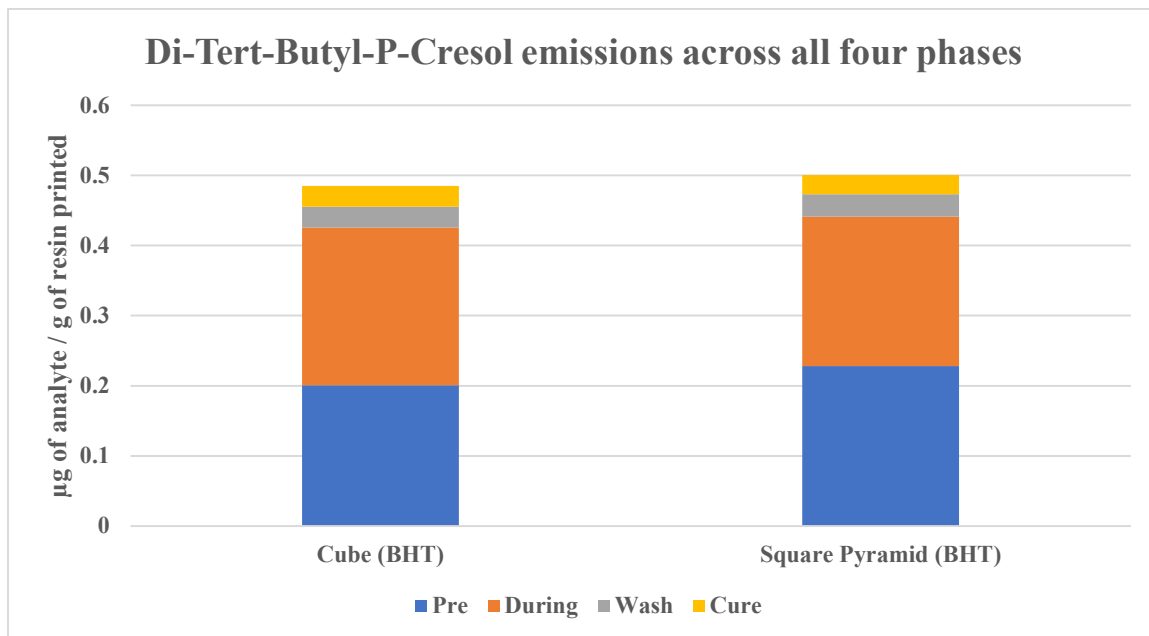


Figure 70: BHT emissions across all four phases. (Plant-based resin)

4-AM was the still the analyte with highest emission, though much lower than that in the oil-based resin. The during phase while the photopolymerization is happening, showed 4-AM in an amount of 55.43  $\mu\text{g}$  per g of resin printed. BHT had the lowest emission in the pre phase, at 0.2  $\mu\text{g}$  per g of resin printed. This is shown below in Figure 71. Figure 72 omits 2-HEA and 4-AM to better present the other four analytes.

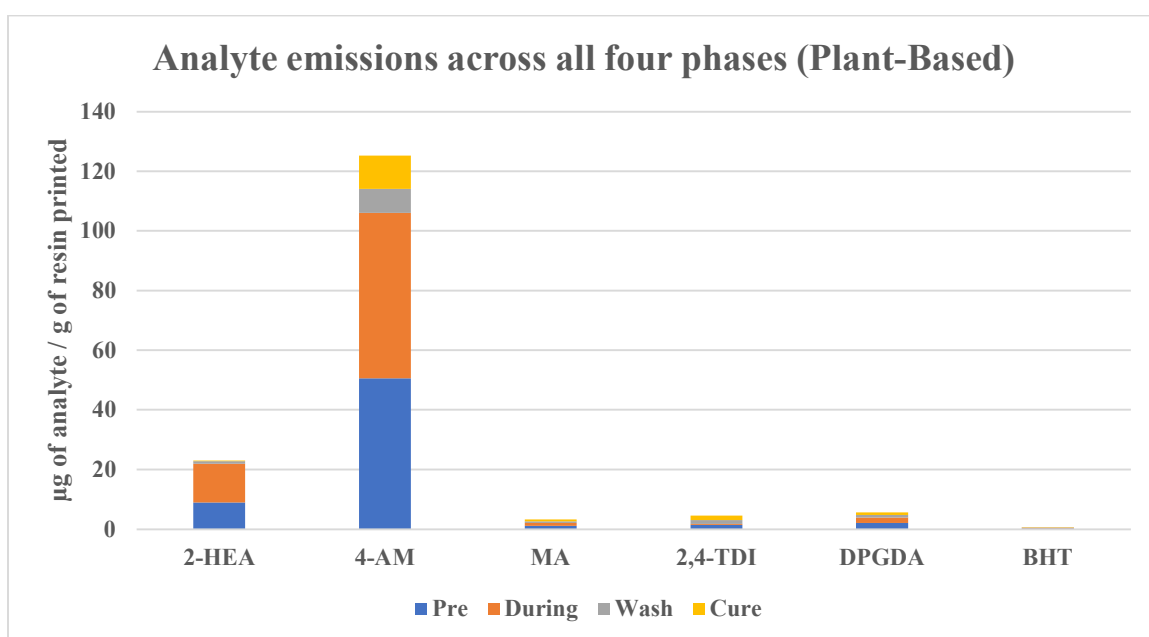
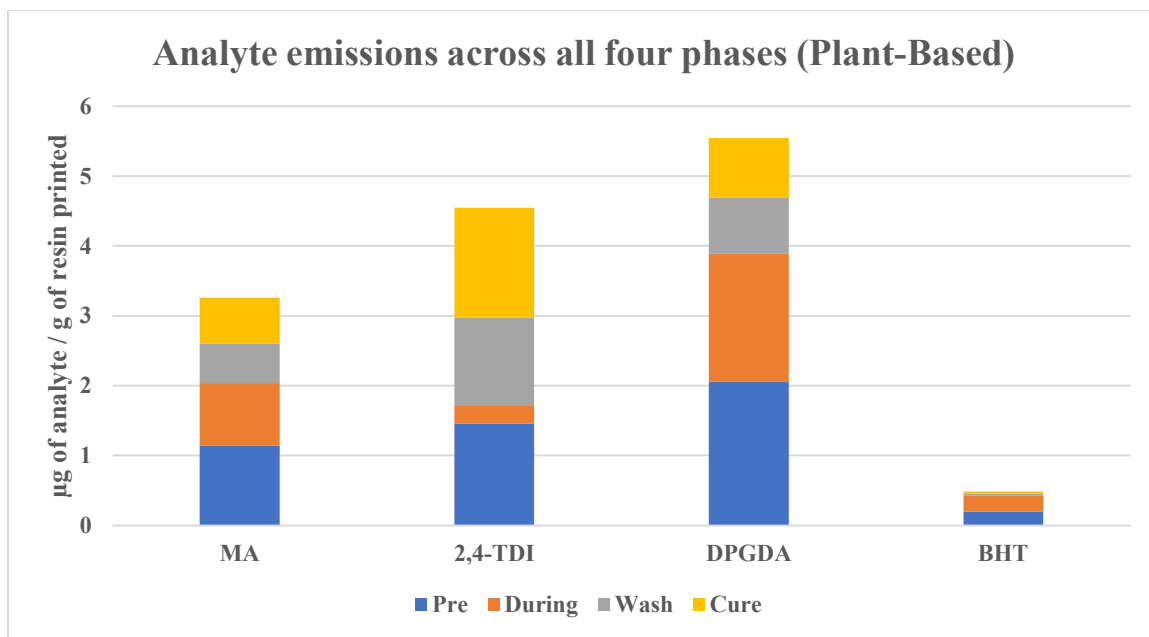


Figure 71: Emissions across all phases for all analytes. (Plant-based resin)



**Figure 72: Emissions across all phases for 4 analytes using the plant-based resin. (2-HEA and 4-AM omitted to emphasize the other four analytes.)**

## 7. DISCUSSION

The presence of the six analytes identified in the resin emission have been chemically justified by indicating their role in the reaction mechanisms presented in chapter 5. The compound concentration across the different phases however is more difficult to rationalize conceptually.

Since the reaction proceeds with exposure to light, the absence of initiation should reduce the emission of the analytes. This however is contrary to the findings presented above. Figure 73 below emphasizes the results, showing the high concentration of VOCs in the pre-phase.

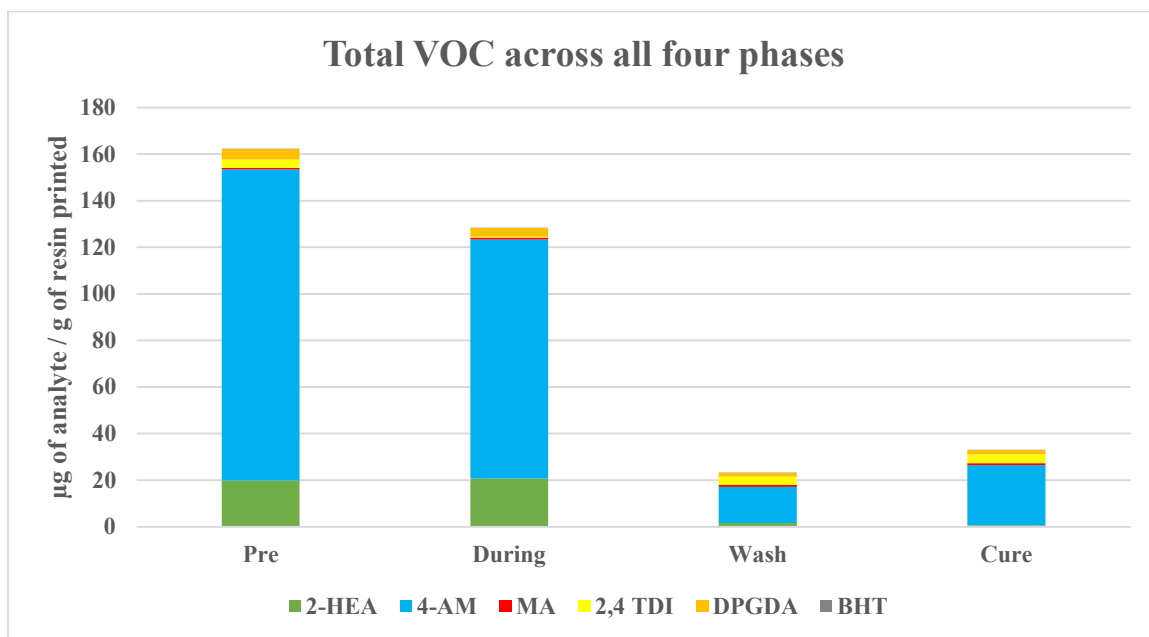


Figure 73: Total VOC across all phases in µg of analyte / g of resin printed.

The pre-phase, when the printer is idle and the resin is not being acted upon by UV exposure, showed the highest concentration of VOCs. There are few plausible reasons for

this, accidental light exposure and spontaneous evaporation. The printer is fitted with UV blocking windows that surround the vat. When the cover of the printer is closed, there is no direct path for light to reach the photopolymer resin. However, there are many reasons that require the lid to be removed: filling the vat, and replacing the build plate being two of the main circumstances. Once a single photoinitiator molecule is radicalized, the polymerization reaction proceeds until a natural slowing caused by lack of light penetration.<sup>30</sup> With this initiation, the analytes of interest could be volatilized. Väisänen et al observed spontaneous evaporation of different photopolymer resins. In the absence of light, increased temperature increased the rate of emission, showing that the reaction can be initiated with different sources of energy (e.g.: heat). Though the work presented in this thesis was done at room temperature, Väisänen et al observed measurable levels of emissions under the same conditions. Table 11 shows emissions for three photopolymer resins before printer-initiated polymerization, two from Väisänen et al and the oil based resin presented in this thesis. Väisänen et al reports their emissions in  $\mu\text{g analyte}/\text{m}^3$ . The size of the area that the printer was contained in was reported to be  $52 \text{ m}^3$  and the model printed was a  $3 \times 3 \times 3 \text{ cm}$  cube ( $31.05 \text{ g}$ ).<sup>13</sup> With this information, the Väisänen results presented in Table 2 can be converted to  $\mu\text{g analyte}/\text{g resin printed}$ , the same units reported in this thesis. The result of this unit conversion compared to results presented in this body of work in Table 11 below. Though the only common analyte is 4-Acryloylmorpholine, 2-Hydroxypropyl Methacrylate and 2-Hydroxyethyl Acrylate are similar in structure giving a strong basis of direct comparison.

Table 11: Compounds detected in three different resins. ( $\mu\text{g}$  analyte/g resin printed). “NM” represents ‘not measured’

Compounds	Clear (Väisänen)	Vero BlackPlus (Väisänen)	Anycubic Clear
2-Hydroxypropyl Methacrylate	10	NM	NM
2-Hydroxyethyl Acrylate	NM	NM	19.1
Isobornyl Acrylate	5.00	2020	NM
4-Acryloylmorpholine	NM	343	134
Propylene Glycol	7.00	559	NM
DPDGA	NM	NM	4.34

Similar to the results found through the procedure detailed in the experimental section, there is a dominant acrylate monomer in the emissions of each feedstocks investigated. This trend follows throughout all four phases.

The high concentration of 4-AM may be explained by fact that resins are made with a proprietary mixture of acrylate monomers in varying composition percentages as shown in the formula below in Figure 74.<sup>31</sup>

2. INGREDIENTS		
Ingredient Name	Composition (Wt%)	CAS No./EC No.
Acrylate Monomer	0%~40%	230-811-7/7328-17-8
Acrylate Monomer	0%~40%	84170-74-1/617-546-6
Acrylate Monomer	0%~40%	51728-26-8/500-111-9
Acrylate Monomer	0%~40%	13048-33-4
Acrylate Monomer	0%~40%	5888-33-5
Acrylated Urethane Polymer	10%~50%	Proprietary
Acrylated Urethane Polymer	10%~50%	68987-79-1

Figure 74: Ingredient list for G3D Clear Resin.

The resin formula includes multiple monomers in various amounts (0%-40%). Since the composition is not explicitly stated, based on Väisänen et al's research and the results presented here, it is probable that one of the monomers is in a higher concentration than the others. With this information, the acrylate composition of the Anycubic Clear and the Anycubic Eco could be predominantly 4-AM, and explain the emission trend observed.

Unsurprisingly, the emissions decrease sharply in the post processing phases. Removing the printer from the enclosure and replacing it with the post processing instrument removes potential emission from the polymerization of the feedstock and leaves the printed object as the primary source of emission. Zhang et al observed this trend of reduction in emission in their work with SLA printers shown below in Figure 75.<sup>12</sup>

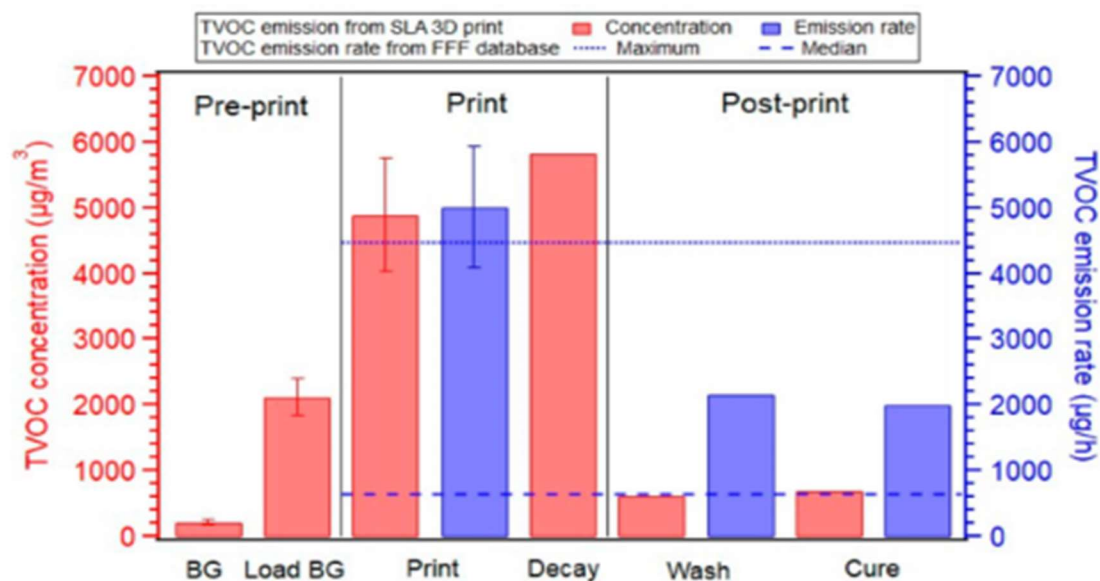


Figure 75: TVOC concentration and TVOC emission rate for an SLA experiment by Zhang et al.

The blue bars in Figure 75 show the TVOC emission rates in  $\mu\text{g}$  analyte/hour. The red bars show the TVOC concentration in each phase, and convey the sharp decrease between the print phase and the post processing phases. This same decrease from pre/print to wash/cure is shown across all of the studies presented in this thesis regardless of printing method.

Though SLA is a different printing mechanism as compared with the mSLA printer used in this work, the post processing method in Zhang et al was done with an instrument nearly identical to the one used in this thesis. Zhang et al reports their emissions in  $\mu\text{g}$  analyte/ $\text{m}^3$  of the chamber. The size of the area that the printer was contained in was reported to be  $1.0 \text{ m}^3$  and the model printed was a  $3.5 \times 3.5 \times 3.5 \text{ cm}$  cube (49.34g).<sup>12</sup> With this information, we can convert their results to  $\mu\text{g}$  analyte/g resin printed, the same units reported in this thesis. The result of this unit conversion compared to results presented in this body of work in Table 14 below. Similar to the data presented in the results section, Zhang et al found 2,6-Di-tert-butyl-p-cresol (BHT) in both the wash and the cure phases. Of note is the trend within those two phases: The final cure emitted a higher concentration of BHT when compared to the wash as shown below.

**Table 12: BHT concentrations of Zhang et al compared to findings in this work ( $\mu\text{g}$  analyte/g resin printed)**

	<b>Wash (Zhang)</b>	<b>Cure (Zhang)</b>	<b>Wash (This Work)</b>	<b>Cure (This Work)</b>
<b>2,6-Di-tert-butyl-p-cresol</b>	0.07	0.12	0.13	0.15

This higher concentration in the cure-phase can be explained by the lack of opportunity for polymerization in the wash phase, spontaneous or otherwise, although the magnitude of the difference is not large. In the cure phase however, the solidified resin is subjected to a final UV exposure that lasted five minutes, providing an opportunity for the reaction to proceed and emit BHT.

### 7.1 OIL-BASED RESIN VS PLANT-BASED RESIN EMISSIONS

Perhaps the most surprising finding of this thesis is the sharp reduction in emissions when comparing the oil-based resin to the plant-based resin. These findings are summarized below in Figure 76 and Figure 77.

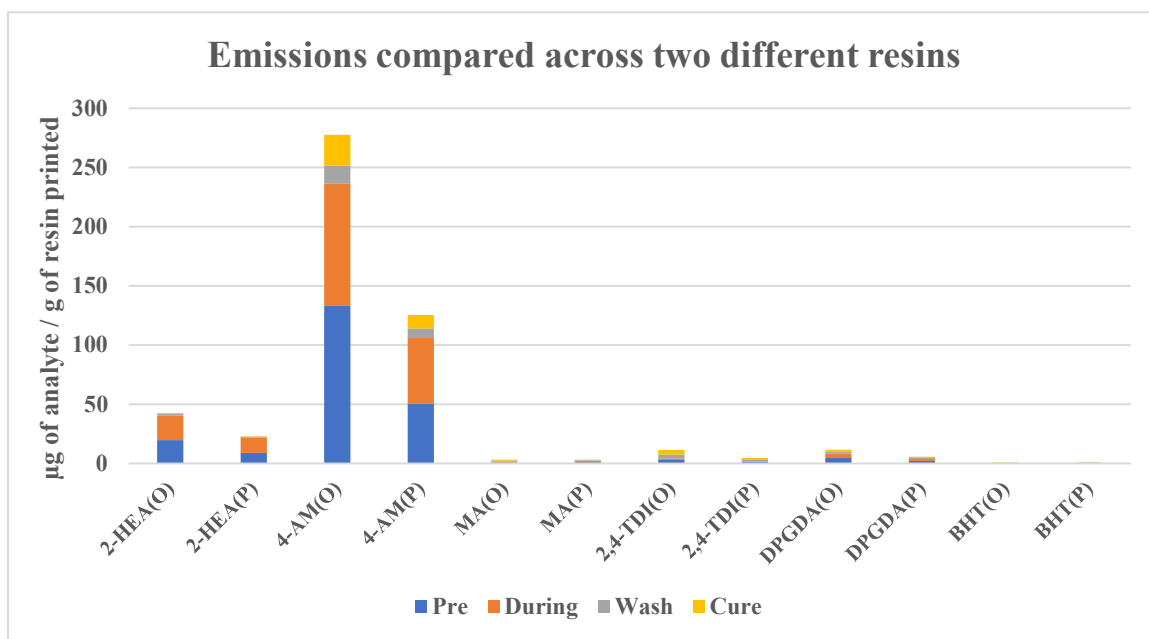


**Figure 76: Comparison of the emissions between the oil-based and plant-based resin experiments.**

(O = Oil-based P = Plant-based)

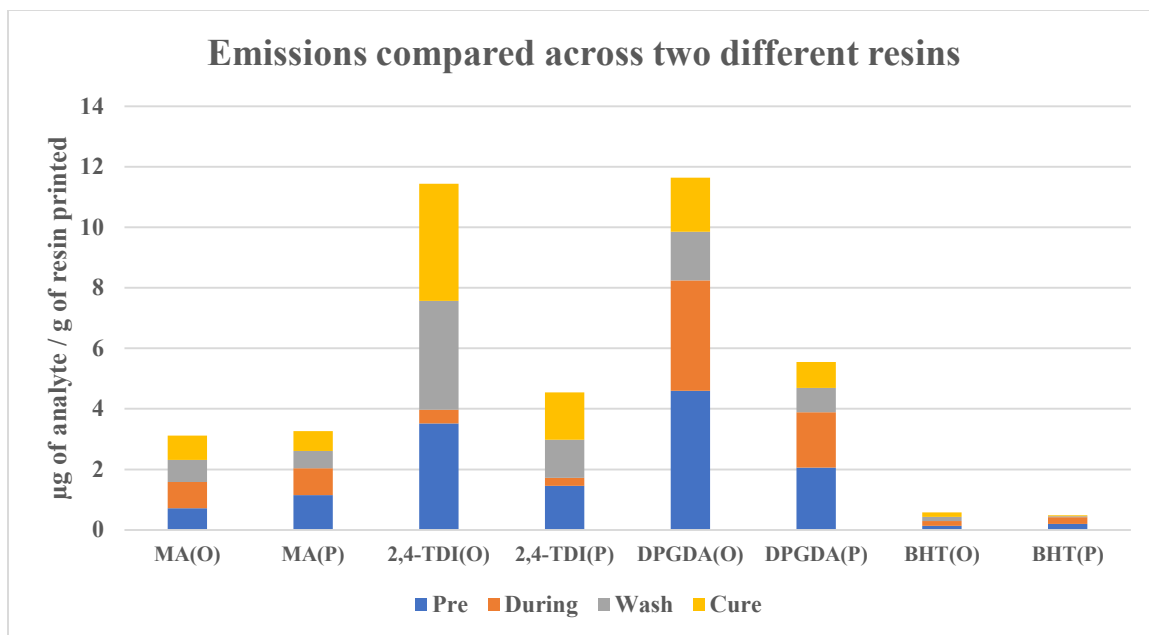


**Figure 77: Comparison of the emissions between the oil-based and plant-based resin experiments. (2-HEA and 4-AM omitted to emphasize the other four analytes.) (O = Oil-based P = Plant-based)**

Conceptually, changing the components of the photopolymer resin would lead to different results. This is seen across multiple studies in the literature: Different resins have varied levels of emission and most of the time completely different identification profiles.<sup>12-14,19</sup> However, in the comparison between the oil-based and plant-based resin, the profile (e.g., GC-FID chromatogram) remained the same and differences were only observed in the concentrations. Figure 78, shows overlapping chromatograms of the analysis of each resin type to emphasize this point. Note that the peaks at 6.3 and 7.6 are almost completely absent in the oil-based, but as shown in the Results section, above the LOD.

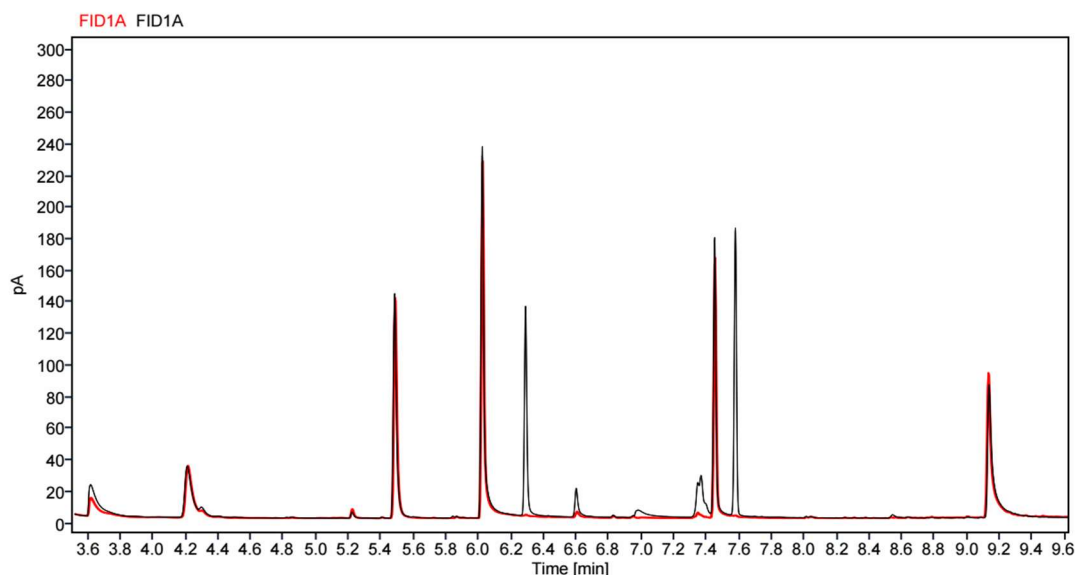


**Figure 78: Overlaid chromatograms of the oil-based and plant-based resin experiments. Black = Oil  
Red = Plant**

According to the manufacturer, the primary difference between the resin formulas is the filler. As discussed in previous sections, the filler is responsible for occupying the space between the polymer chains and imparting the unique physical properties and avoid unfavorable properties such as shrinkage, brittleness and sluggish photocuring.<sup>29</sup> While no fillers were identified in the analysis presented in this thesis, that does not indicate an absence thereof. There is a possibility that these components are not easily volatilized and therefore absent in our study. Though we cannot measure non-volatile components with our experimental design, there is an explicit difference in the concentration of the 6 VOCs we monitored with no apparent difference in the final product. With this in mind, it is accurate to state that outside of the filler content, there is a broad reduction in VOCs from oil-based to plant-based resin feedstock.

The effects of exposure to the six VOCs measured here analytes are an important point in the discussion of difference between the oil-based resin and the plant-based resin. The GHS hazard codes assigned to the identified analytes are consolidated below in Table 13.<sup>32</sup>

**Table 13: Hazard Statements associated with all six analytes condensed.**

<b>H-Code</b>	<b>Hazard Statement</b>
<b>H311</b>	Toxic in contact with skin
<b>H314</b>	Causes severe skin burns
<b>H315</b>	Causes skin irritation
<b>H 317</b>	May cause an allergic skin reaction
<b>H318</b>	Causes serious eye damage
<b>H319</b>	Causes serious eye irritation
<b>H330</b>	Fatal if inhaled
<b>H334</b>	May cause allergy or asthma symptoms or breathing difficulties if inhaled
<b>H335</b>	May cause respiratory irritation
<b>H351</b>	Suspected of Causing cancer
<b>H373</b>	Causes damage to organs through prolonged exposure
<b>H400</b>	Very Toxic to Aquatic Life
<b>H410</b>	Very toxic to aquatic life with long lasting effects
<b>H412</b>	Harmful to aquatic life with long lasting effects

Of all of the hazard statements presented above, perhaps the most concerning is H330 (Fatal if inhaled) and the response precautionary statements P304, P316 (If inhaled, get emergency medical help immediately.) Only one compound has been assigned this hazard statement, 2,4-TDI. If used as a basis of measurement for safety, the two-fold reduction in 2,4-TDI emission in the plant-based resin is a clear indicator of it being a safer feedstock without any observable difference in the mechanical properties imparted by the

difference in filler material. As none of the other five VOCs were more abundant in the plant-based resin as compared with the oil-based resin, this appears to be a safe assumption.